Computers and Electronics in Agriculture 243 (2026) 111378

Contents lists available at ScienceDirect

Computers and Electronics in Agriculture

journal homepage: www.elsevier.com/locate/compag

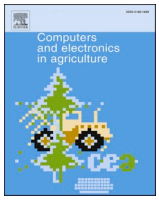

Review Article

Accuracies and costs of prediction and mapping soil properties using proximal sensors: A systematic review

Carlos Lozano-Fondón [a], Romina Lorenzetti [b,*], Roberto Barbetti [c], Konrad Metzger [d], Gabriele Buttafuoco [e], Melis Özge Pinar [f], Sevinç Madenoğlu [g], Taru Sandén [h], Asa Gholizadeh [i], Bo Stenberg [j], Maria Fantappiè [a], Fenny van Egmond [k], Frank Liebisch [l], Rafael López Núñez [m], Maria Knadel [n], Triven Koganti [n]

[a] Research Centre for Agriculture and Environment, Council for Agricultural Research and Economics, via di Lanciola 12/A, 50125 Florence, Italy
[b] CNR-IBE, Institute of BioEconomy, National Research Council of Italy, Area della Ricerca di Firenze, Via Madonna del Piano, 10, 50019 Sesto Fiorentino, Italy
[c] Research Centre for Forest and Wood, Council for Agricultural Research and Economics, Strada Frassineto, 35, 15033 Casale Monferrato, Alessandria, Italy
[d] Agroscope, Field-Crop Systems and Plant Nutrition, Route de Duillier 60, 1260 Nyon, Switzerland
[e] National Research Council (CNR) of Italy, Institute for Agricultural and Forest Systems in the Mediterranean Via Cavour 4/6, 87036 Rende (CS), Italy
[f] Ministry of Agriculture and Forestry, Transitional Zone Agricultural Research Institute, Eskişehir, Turkey
[g] Ministry of Agriculture and Forestry, General Directorate of Agricultural Research and Policies (TAGEM), Ankara, Turkey
[h] Department for Soil Health and Plant Nutrition, Austrian Agency for Health and Food Safety (AGES), Spargelfeldstrasse 191, 1220 Vienna, Austria
[i] Department of Soil Science and Soil Protection, Faculty of Agrobiology, Food and Natural Resources, Czech University of Life Sciences Prague, Prague, Czech Republic
[j] Department of Soil and Environment, Swedish University of Agricultural Sciences (SLU), Skara, Sweden
[k] Wageningen University and Research, Wageningen, the Netherlands
[l] Agroscope, Water Protection and Substance Flows, Reckenholzstrasse 191, 8046 Zürich, Switzerland
[m] Instituto de Recursos Naturales y Agrobiología de Sevilla, IRNAS-CSIC, Avenida Reina Mercedes 10, 41080 Seville, Spain
[n] Department of Agroecology, Aarhus University, Blichers Alle 20, 8830 Tjele, Denmark

ARTICLE INFO

Keywords:
Electromagnetic sensors
Covariates
Data fusion
Precision agriculture mapping
Cost analysis
Soil
Sensing
Proximal

ABSTRACT

This review provides an overview of the accuracy of soil property predictions using the most common proximal soil sensing (PSS) techniques in precision agriculture (PA), both standalone and in combination with one another or with environmental covariates. Based on 114 scientific papers, the accuracy of soil property estimates was evaluated by calculating the normalized root mean square error (NRMSE) using root mean square error (RMSE) values and the range of the predicted soil property. Soil properties, PSS techniques, covariate types, and the type of model employed for predictions were the factors around which accuracy results were sorted. Additionally, we estimated PSS service costs based on both the literature and on a market study with questionnaires for private companies operating in the PA sector. Our literature analysis indicates that diffuse reflectance spectroscopy (DRS) was able to estimate the greatest number of soil properties with a high accuracy compared to the other PSS techniques. The most popular applications of DRS are to determine soil organic matter, nutrients, and soil texture, although most of the applications are primarily lab-based. X-ray fluorescence (XRF) is the second most popular technique for soil property estimation; however, in contrast to DRS, most estimations are in-field applications with portable XRF sensors. The use of XRF is widespread in determining elemental concentrations. On-the-go techniques such as electromagnetic induction (EMI) or gamma-ray spectroscopy (γ-ray) accounted for lower accuracy compared to point-based techniques (e.g., DRS, XRF, time-domain reflectometry). However, they are widely used by companies, as they have vast potential to delineate PA management zones in the field, and are suitable for on-the-go mapping of soil properties such as mineralogy, texture, salinity, water content, cation exchange capacity, and soil depth. The combined use of PSS techniques generally doesn't outperform the singular application, although the number of samples collected for calibration, and specific combinations of sensors, covariates, and modeling techniques, combined correctly, may enhance the predictions of soil properties using PSS techniques applied singularly. However, these outcomes tend to depend on local site characteristics. Differences were found between the analysis of costs collected from the literature and from the companies' survey. The estimated cost of surveying a hectare with PSS oscillates between 15.5€/ha and 130€/ha, according to

* Corresponding author.
E-mail address: romina.lorenzetti@cnr.it (R. Lorenzetti).

https://doi.org/10.1016/j.compag.2025.111378
Received 16 September 2025; Received in revised form 19 December 2025; Accepted 23 December 2025
Available online 5 January 2026

research data, whereas our company survey resulted in an interval between 142 and 362€/ha. Price variability was influenced by personnel costs, fieldwork, data and reporting, sample analysis, and equipment. Besides, increases in the final prices can be attributed to accessibility and difficulties related to field work, as well as traveling to the area of interest. This review aims to serve as a reference for encouraging the adoption of current and available sensing technologies by farmers, policymakers, and companies by providing helpful insights into the suitability of different PSS techniques for mapping various soil properties, their associated costs, and what is available in the market. We foresee that availing PSS services will become cheaper with technological advances. Thus, it will become a standard approach in the future, as it is the most feasible way for producing high-resolution maps and affordable soil property information.

1. Introduction

Accounting for spatial and temporal variability of soil properties is central in the context of precision agriculture (PA), particularly for improving the sustainability of production (Kerry and Escolà, 2021). Many sources of variation at the field scale influence soil-forming factors and derived soil properties (Oliver, 2010; Goovaerts, 2017). Therefore, the adoption of PA for site-specific management requires high spatial and temporal resolution of soil information (Gebbers and Adamchuk, 2010). However, conventional analytical procedures involving invasive field sampling are cost-intensive and often do not meet the spatial resolution required by PA. Reliable quantification of soil properties is necessary to gain confidence in the results. Thus, several international organizations (ISO, CEN, USEPA) have developed standardized measurement protocols for various soil health properties in specific contexts, such as agriculture (Nortcliff 2002; Perčin et al., 2025). However, the physical and chemical target soil properties are usually determined using classical wet chemistry analytical procedures. These procedures have a set of characteristics that, in general, make them slow and expensive due to the need for trained personnel, specialized equipment, laborious sample preparation, the use and disposal of waste of sometimes toxic or hazardous chemicals, and the need for extensive laboratory space.

The requirement of high temporal and spatial resolution data for PA can be effectively fulfilled through different proximal soil sensors and sensing modalities (Viscarra Rossel et al., 2010; Viscarra Rossel and McBratney, 1998). Indeed, the rapid technological advancements from the Second World War to the 21st century in fundamental physics have enabled the development and availability of tools for proximal soil sensing (PSS), which have also become feasible to use and affordable over time and leading (Fig. 1), for example, to a rise in their use in the scientific literature (Viscarra Rossel et al., 2010; Viscarra Rossel et al., 2011; Adamchuk et al., 2021; Barra et al., 2021; Piccini et al., 2024). From the late 1990s and especially since the early 2000s, PSS technologies have progressively shifted from laboratory-based instruments toward portable, in situ and on-the-go sensing platforms, enabling real-time, high-resolution mapping of soil properties directly in the field. The scientific literature clearly demonstrates how PSS applications can yield quantitative results more efficiently and cost-effectively than traditional laboratory analyses (Fig. 2). Although sensors are becoming increasingly smaller, faster, more accurate, and more energy-efficient (Aarif et al., 2025), costs associated with different PSS techniques should be carefully considered and weighed against the accuracy they provide for various soil properties. In fact, PSS methods enable the collection of information in the proximity of soil by measuring parts of the electromagnetic spectrum after radiation interacts with the soil volume (Piccini et al., 2024), but this occurs at the expense of the accuracy that can be achieved in traditional wet chemistry measurements of soil properties. Therefore, planning which PSS methods to apply and the number of conventional analyses to perform for calibration is crucial during PSS surveys.

Over the years, different sensing modalities have been proposed: 1) invasive or non-invasive, if the sensor is inside or outside the measurement volume; 2) active or passive if the system includes an external energy source or not; 3) mobile or stationary depending on whether the system is capable of measuring in motion or only in stationary mode (McBratney et al., 2011a; Piccini et al., 2024). As mentioned above, PSS techniques rely on proxies to determine the existing relationship between specific parts or windows of the electromagnetic spectrum and soil properties of interest. This requires the use of calibration and validation data sets and modelling procedures to accurately estimate the properties (Sudduth et al., 2001).

Modelling approaches in proximal soil sensing require mathematical or statistical treatments to extract useful information and relate the traditional measures of the soil constituents or properties to the proximally sensed data. Such treatments, in the early period (1980s to 1990s) until about 2010, resulted in different multivariate approaches, which over the past three decades, have strongly evolved from linear assumptions of the relation between proximally sensed data and traditional laboratory measured data to non-linear and more complex purely data-driven modelling. Using as an example diffuse reflectance spectroscopy, the mathematical approaches, known as chemometrics, have evolved from using specific wavelengths selected by methods of stepwise regression to using full high-resolution spectra in multiple linear regression (MLR), principal components regression (PCR) and partial least-squares regression (PLSR) to handle collinearity in high-dimensional spectra (Stenberg et al., 2010; Næs et al., 2004; 2010). However, they all continued to assume mostly linear relationships. As sensor technologies advanced and datasets expanded, a rapid evolution of approaches are being made available thanks to the application of machine learning (ML) methods in soil science (Minasny and McBratney, 2025) from about 2005 to the present. Among these approaches are non-linear algorithms such as random forest (RF), support vector machine regression (SVMR), and artificial neural network (ANN), and many others (James et al., 2021; Minasny and McBratney, 2025).

Progress in soil mapping is documented in the review by Gomes et al. (2023), with experience from Denmark demonstrating practical applications. The work explored mapping soil functions using soil information collected from multiple sources, including conventional data, PSS data on several platforms, and the use of covariates (e.g., high-resolution variables such as climate, relief, parent material, and soil properties and attributes, among others). Besides, it analyzed the impact of rapidly advancing modeling techniques, such as machine and deep learning, on the production of digital soil maps (DSM). The relevance of non-linear modelling when working with PSS data contributes to enhancing the level of reliability, precision, and resolution of spatial models of soil properties. This, in fact, can provide meaningful insights and facilitate effective decision-making, anticipate forthcoming alterations, and advise strategies for future challenges in agriculture. In addition, the EU Soil Monitoring and Resilience Law (Directive (EU) 2025/2360, 2025) indicates the need to use validated transfer functions when methods for determining properties other than the standardized reference methods in the Law are employed. As such, the Law points to the need to harmonize calibration and/or validation data and to the possibility to use alternatives to wet chemistry, if the quality, reliability and transformability of results to values as would have been provided by reference methods are proven.

Simultaneously with the increase in publications about PSS, many

Fig. 1. Development and evolution of proximal soil sensing (PSS) in the context of precision agriculture (PA).

companies are adopting these technologies, and startups offering PSS services to farming communities are emerging. To our knowledge, several important reviews on PSS have been published, including those by Viscarra Rossel et al. (2011) and Adamchuk et al. (2018). However, an updated, exhaustive review of all proximal techniques used in the context of PA to assess soil health-related indicators is missing. Moreover, to our knowledge, none of the existing reviews explicitly combine a cross-technique synthesis of quantitative prediction accuracy (e.g., NRMSE) with a systematic comparison of cost ranges, which is essential for supporting practical sensor selection and deployment decisions. In particular, a focus on the reliability of quantitatively measured soil property predictions and on the costs associated with the use of specific techniques, platforms, and covariates classified by soil property would provide a more complete overview of the topic that can be used by practitioners and other users. Therefore, the general aim of this work is to provide an updated framework for selecting the most suitable and accurate PSS technique for predicting fundamental soil properties in the context of PA, based on a thorough literature review of accuracy and a company cost survey. Although this review is the product of the ProbeField project, and for this reason it is intended to be focused on proximal soil sensing techniques implemented within the project, other emerging PSS approaches are qualitatively addressed, mainly as future perspectives. Specifically, the objectives were set as follows: 1) to provide a technical framework and principles of the PSS techniques under review; 2) to provide a comprehensive overview of the accuracies achieved in the literature depending on the PSS technique and sensor's response, used alone or in combination with others, 3) to analyze and account for the effect of other factors involved in soil properties prediction, and 4) to evaluate the cost associated with the use of PSS in academia through the literature review, and in the market through the analysis of the answers to questionnaires from PSS companies operating in the private sector.

2. Proximal sensing techniques under review

The technical characteristics of electromagnetic sensors determine their sensitivity to specific parts or windows of the electromagnetic spectrum (Fig. 3). Depending on the frequency, electromagnetic sensors can provide indirect information about the soil itself and its forming components (McBratney et al., 2003; Viscarra Rossel et al., 2010, 2011).

2.1. Diffuse reflectance spectroscopy (DRS)

Visible near-infrared (vis-NIR) and mid-infrared (MIR) diffuse reflectance spectroscopy (DRS) are analytical techniques that operate in the wavelength ranges of 350–2500 nm and 2500–25,000 nm, respectively. These methods measure the energy reflected by a material, such as soil, when exposed to electromagnetic radiation (Duda et al., 2017). The apparent absorption is estimated from what is not reflected in relation to a known, typically white, reference reflection. While MIR absorption is associated with fundamental molecular vibrations, vis-NIR absorption corresponds primarily to overtones and combination bands (Williams & Norris, 2001). Spectral data are acquired using spectroradiometers, which produce known spectra of reflectance or absorbance as a function of wavelength. Spectral absorption arises primarily from molecular bond vibrations, such as bending, stretching, and twisting, and the absorption band for a specific bond in one particular compound, related context, or matrix corresponds to the required energy quantum

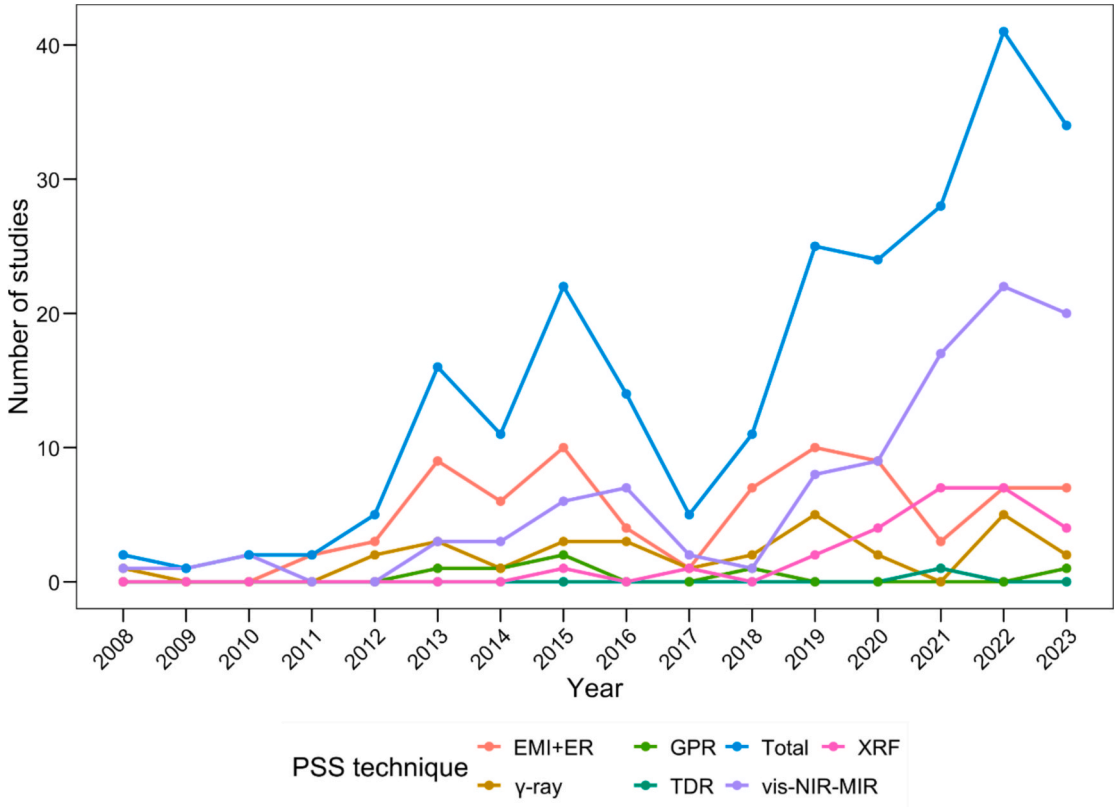

Fig. 2. Number of publications (n = 243) between 2008 and 2023 found on the Scopus database using the keywords "Proximal soil sensing" and the class of "proximal sensor" for different proximal sensing technologies (colors). The development of portable spectrometers operating in the vis-NIR-MIR contributed considerably to the total number of investigations carried out in proximal soil sensing (PSS). At the same time, the application of other electromagnetic techniques, such as γ-ray, EMI, and XRF, varied over the years. Investigations that apply TDR and GPR techniques to soil remained stable despite their potential in water management. DRS: diffuse reflectance spectroscopy; γ-ray: gamma-ray spectroscopy; EMI/ER: electromagnetic induction/electrical resistivity; TDR/FDR: time-domain reflectometry/frequency-domain reflectometry; XRF: X-ray fluorescence; LM: linear modeling; NLM: non-linear modeling.

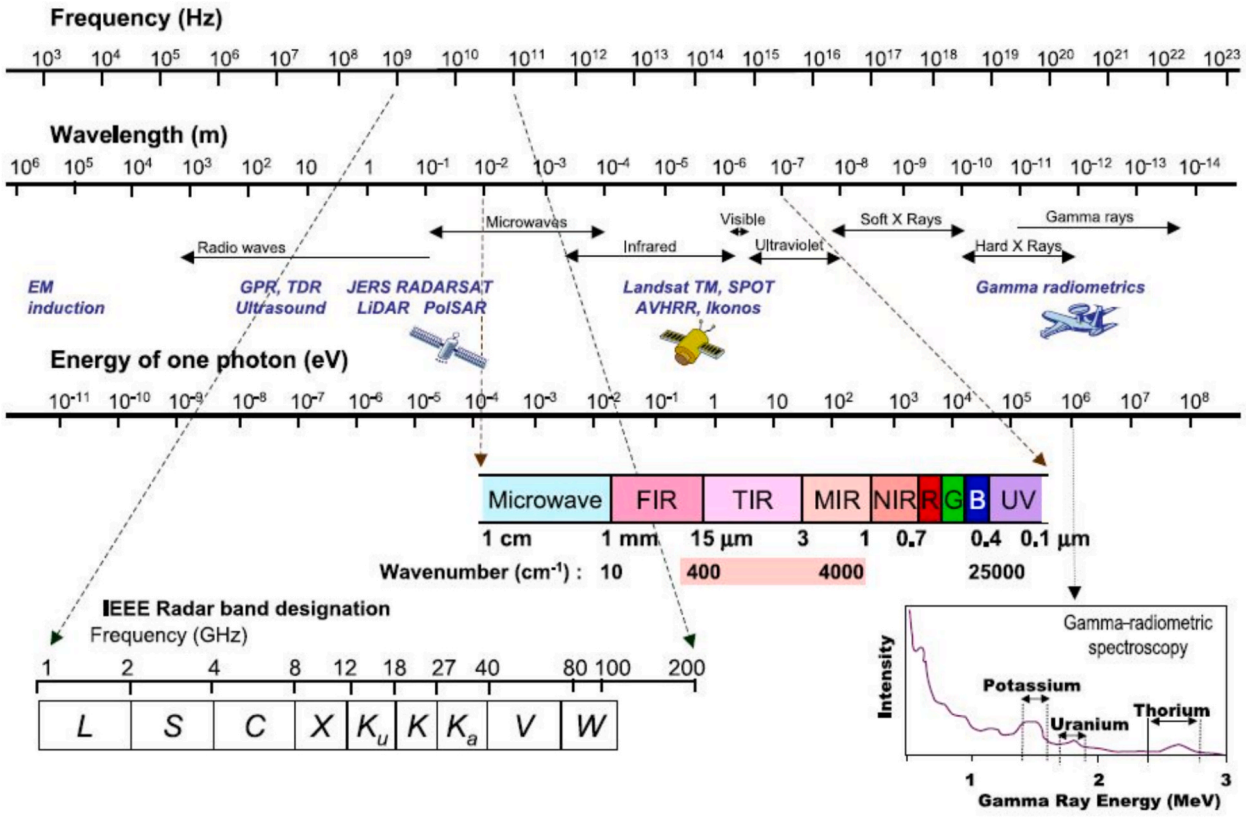

Fig. 3. The electromagnetic spectrum showing the frequency ranges of different proximal and remote sensors (from McBratney et al., 2003).

causing a specific molecular vibration. Both organic matter and clay minerals (and other minerals ending up in the clay fraction) have several characteristic absorption features across this spectral region (Stenberg et al., 2010; Wetterlind et al., 2022).

DRS is highly sensitive to physical factors such as particle size, aggregation, and moisture, which can significantly affect reflectance (Cascante et al.,2025; Chang et al., 2011; Liu et al., 2003; Knadel et al., 2023; Stenberg, 2010). Although MIR was initially deemed unsuitable for quantifying absolute concentrations due to its sensitivity to sample heterogeneity (Niemeyer et al., 1992), subsequent research has demonstrated successful estimations of elemental concentrations using both laboratory-based and handheld instruments (Bellon-Maurel and McBratney, 2011; Clairotte et al., 2016).

By analyzing spectral signatures, soil properties and types can be characterized and element concentrations can be estimated, using chemometric approaches that link spectral data with reference measurements through multivariate regression, machine learning, or deep learning. However, several sources of uncertainty—such as sensor design, spectral calibration references, sample preparation, and spectral preprocessing—can impact model performance and require careful validation (McBride, 2022). To ensure comparability across studies, it is essential to quantify measurement uncertainty and adopt standardized evaluation procedures (Sudduth and Hummel, 1996; Brodsky et al., 2013). Protocols such as the International Soil Standard (ISS) for laboratory spectral alignment (Ben-Dor et al., 2015) and field measurement guidelines (Stenberg et al., 2024) are recommended to address variations related to instrument configuration and environmental acquisition conditions.

A valuable application of spectroscopy is soil spectral libraries (SSLs), which are collections of soil reflectance spectra (usually in either the vis-NIR-SWIR or the MIR ranges), along with reference soil property data (e.g., organic carbon, texture, nutrients). These libraries serve as calibration databases that enable rapid, non-destructive prediction of soil properties using spectral models. They can be local (specific to a region or study) or global, such as the USDA's NRCS-KSSL library or the FAO–ISRIC Global Soil Spectral Library. See Brown et al. (2006), Viscarra Rossel et al. (2016), Sanderman et al. (2019) and Ramírez-López et al. (2019) for further details.

2.2. Electromagnetic induction (EMI)

The EMI technique operates in the low-frequency (~ 1–100 kHz) radio wave region of the EM spectrum. In this technique, conduction currents are the dominant energy transport mechanism (Everett 2013a), and the method is primarily used to measure the bulk electrical conductivity (EC) of a soil volume. While many variants exist, the frequency-domain instruments called ground conductivity meters are most commonly used in agricultural applications.

Corwin and Lesch (2003) show the evolution, theory, applications, and guidelines of instruments measuring soil EC. For instance, authors noted that in the 1970s, four-electrode arrays were used to measure EC, which later evolved into a tractor-mountable fixed array in the 1990s. At present, instruments mounted behind an ATV are typically used (e.g., Veris, Geophilus). In parallel, the EMI instrument became popular with the advent of Geonics EM38 for soil mapping in the 1980s. At present, single-transmitter multireceiver (e.g., DUALEM, CMD) and multifrequency (GEM2) instruments are commonly used.

A typical EMI instrument consists of a Transmitter (Tx) and one or multiple receiver (Rx) coils. An alternating current (AC) induces a transient primary magnetic field into the ground by powering the Tx coil (Fig. 4). This primary field generates eddy currents depending on the EC of the subsurface, which generates a secondary magnetic field. While the receiver coil measures both the primary and secondary fields, the secondary field can be distinguished because the primary field can be estimated based on the Tx-Rx configuration. Generally, the secondary field is delayed and attenuated in comparison to the primary field, and

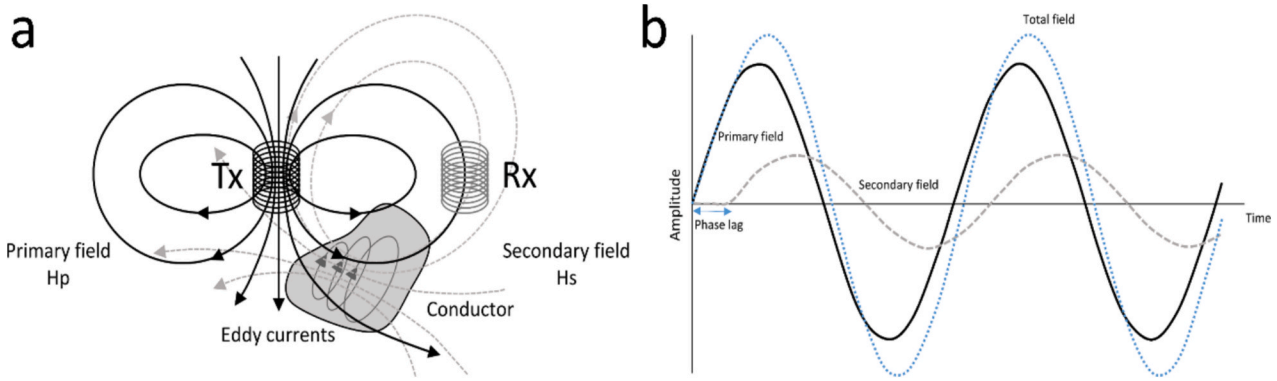

Fig. 4. Schematic diagram showing the working principle of an electromagnetic induction instrument: (a) processes that lead to the generation of the secondary magnetic field and (b) phase lag between the primary and secondary fields that facilitates the quantification of the apparent electrical conductivity.

the phase lag depends on the bulk soil EC. The secondary field occurs completely out-of-phase, if the ground is perfectly conductive, and in-phase, if the ground is perfectly resistive. The total field can be decomposed into real (in-phase) and quadrature (out-of-phase) responses, with the former indicating the apparent magnetic susceptibility and the latter representing the apparent EC (EC_a) of the subsurface.

The sensitivity and depth of exploration (DOE) of ground conductivity meters depend on the Tx-Rx coil orientations (Fig. 5) as well as the spacing between them (McNeill, 1980; Abdu et al., 2007; Saey et al., 2009). For example, the commonly used EM38 (Geonics Ltd., Mississauga, ON, Canada) variant with a one-meter Tx-Rx separation can be either employed in the horizontal coplanar (HCP) mode with a DOE of 1.6 m or by rotating the instrument by 90 degrees, forming the vertical coplanar (VCP) mode with a DOE of 0.75 m. Increasingly, on-the-go measuring instruments with multiple Rx coils at different spacings from the Tx coil, such as DUALEM (DUALEM Inc., Milton, ON, Canada) with HCP and perpendicular (PRP) modes, are becoming more common. Alternatively, different depth sensitivities can also be achieved using instruments that operate on multiple frequencies, for example, GEM-2 Ski (Geophex Ltd., Raleigh, NC, USA).

The EMI instruments are extensively used in the agricultural and land management sectors for mapping soil properties, particularly soil salinity, texture, and water content (Huang et al., 2017; Pedrera-Parrilla et al., 2016), as well as delineating management zones (Hedley et al., 2004; Corwin and Lesch, 2003).

Additionally, EMI instruments can be configured to measure magnetic susceptibility (MS) and be applied in several contexts, such as soil texture predictions, determination of heavy metal content, and evaluation of irrigation water quality (Yang et al., 2007). The methodological framework for how MS is measured in soil can be found in Shirzaditabar and Heck (2022), whereas Ramos et al. (2021) note that MS shows strong linear correlations with physical, chemical, and mineralogical soil attributes (e.g., sand and clay contents) and can help delineate soil boundaries due to lithological and pedological variation.

2.3. Gamma (γ) ray spectroscopy

Gamma-ray spectroscopy measures the intensity distribution of gamma radiation (γ) as a function of the energy of individual photons naturally emitted by low radioactive elements or radionuclides in matter such as soil, the geological substrate or buildings, through atomic decay processes. Gamma rays are a highly energetic form of electromagnetic radiation. Expressed in kiloelectron volts (keV), they are characterized by extremely high frequencies ($<10^{20}$ Hz) and very short wavelengths ($>10^{-11}$ nm). These properties confer a strong ionizing capacity ($>10^{6}$ eV), enabling gamma radiation to interact effectively with matter.

Traditional γ-ray radiometers employ scintillation crystals such as sodium iodide (NaI), which, when coupled with a photomultiplier tube, can detect and quantitatively measure gamma radiation that passes through the crystal. Although NaI crystals are widely used, they are not the most efficient in capturing γ radiation. Commercially available alternatives include bismuth germanate ($Bi_4Ge_3O_{12}$, also known as BGO) and cesium iodide (CsI), both of which offer higher detection efficiencies, which means the size of the crystal can be smaller compared to NaI. Another difference between the crystals is their brittleness, e.g. BGO is more brittle than CsI and NaI. However, they typically exhibit lower energy resolution, potentially limiting their use in applications that require accurate radionuclide identification if peak identification is used as analysis method. Typical spectral analysis methods are the Windows method and the Full Spectrum Analysis method (Van der Graaf et al., 2007; Van Egmond et al., 2010). The first one uses the known location of energy peaks and estimates the concentration based on the height of the peak. The latter uses the full spectral fingerprint of the gamma radiation of a single radionuclide to estimate the concentration

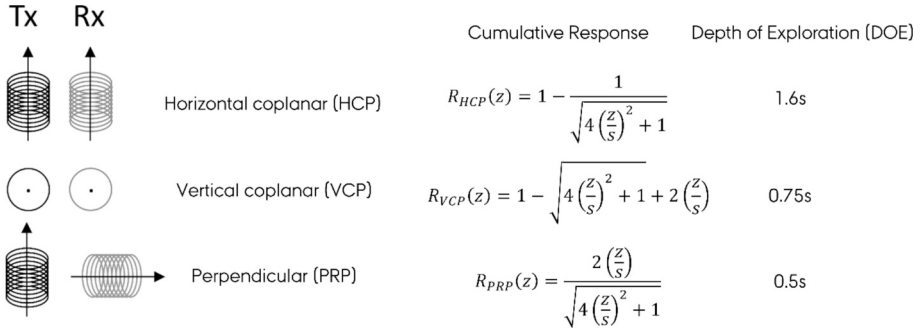

Fig. 5. Schematic diagram showing the different possible transmitter (Tx) and receiver (Rx) coil arrangements with corresponding cumulative response functions and depths of exploration. 'z' and 's' correspond to the depth and coil separation between the Tx and Rx coils, respectively. Please refer to Abdu et al. (2007) and Saey et al. (2009) for further details.

of occurring radionuclides through a least squares analysis.

Gamma-ray (Van der Graaf et al., 2007) sensors can be classified into two categories: active and passive. Active γ sensors are increasingly used to estimate additional soil properties, such as bulk density, by measuring backscattered γ radiation from a low-activity source (Pepers et al., 2024). They are typically employed on a stick that is lowered in the ground, generally to a depth between 10 and 60 cm, after preparing a small borehole or by extracting the soil core and measuring the core in the field or lab. This approach expands the utility of γ-ray sensing beyond radionuclide mapping to broader applications in soil physics. For mobile applications such as precision agriculture, passive sensors mounted on vehicles or carried manually are generally preferred (Viscarra Rossel et al., 2007). These systems facilitate the detection of radionuclide contributions from isotopes such as ^{40}K, ^{238}U, ^{232}Th, and ^{137}Cs. While ^{40}K, ^{238}U, ^{232}Th are naturally occurring radionuclides, ^{137}Cs is of anthropogenic origin, introduced into the environment by the Chernobyl disaster in 1986 and nuclear weapons testing worldwide since the 1950s. By quantifying gains or losses of ^{137}Cs at the soil surface, researchers can estimate rates of soil erosion (Fulajtar et al., 2017; Porto et al., 2024). Furthermore, the spatial distribution of radionuclide counts has been correlated with various soil properties, including soil texture, moisture content, and mineralogical composition to an average depth between 30 and 50 cm.

Radionuclide concentrations are typically expressed in becquerels per kilogram (Bq/kg). At the surface, detectable γ radiation for passive sensors originates from the upper 30 cm of soil, as deeper signals are attenuated by overlying dry soil and moisture content (Cook et al., 1996; Viscarra Rossel et al., 2007). Strong correlations have been observed between ^{232}Th levels and clay content in topsoil, particularly in studies conducted in the Netherlands (Van Egmond et al., 2010) and Sweden, where aerial gamma radiometry was one of the key features for a national digital soil map (Piikki and Söderström, 2019). Other research has identified significant relationships between radionuclide distributions and both physical (e.g., texture, grain size) and chemical soil properties (e.g., heavy metal contamination, fertilizer application, nutrient levels) (van der Graaf et al., 2007; Viscarra Rossel et al., 2007). In Sweden, a combination of aerial and ground-based γ-ray spectrometry (^{238}U, ^{232}Th, and ^{40}K), combined with maps on bedrock geology and Quaternary soil deposits, was used to identify agricultural land with risk for elevated levels of cadmium in crops (Söderström and Eriksson, 2013).

2.4. Dielectric methods

Soil dielectric constant ε (aka relative dielectric permittivity (RDP)) is a key property for predicting soil volumetric water content (Topp et al., 1980) and soil texture layering. The RDP is a measure of a material's polarizability, i.e., a material's ability to store and release electromagnetic (EM) energy and control the EM wave velocity. Its value depends on both the induced polarizability and the angular frequency ω of the imposed electric field (White and Zegelin, 1995). In soils, the RDP values often reflect the amount of water content, as water is highly polarizable (RDP ~ 81), whereas air and mineral components have RDP values of around 1 and 3, respectively. For example, the wet sands have RDP between 15 and 30, whereas the dry sands have RDP between 4 and 6 (Cassidy, 2009). Moreover, this significant difference in the dielectric constant of water and soil solid constituents makes the method relatively insensitive to soil composition and texture (Jones et al., 2002).

The bulk dielectric constant of soil infers the volumetric soil water content (θ_v) by using empirical relationships. The most widely used for agricultural soils is the empirical model developed by Topp et al. (1980):

$$\Theta_v = \left(5.3\times10^{-2}\right) + \left(2.29\times10^{-2}\right)\varepsilon_b - \left(5.5\times10^{-4}\right)\varepsilon_b^2 + \left(4.3\times10^{-6}\right)\varepsilon_b^3 \quad (1)$$

It is a third-order polynomial, considered valid for relating soil volumetric water content (θ_v) and bulk dielectric constant (ε_b) for most mineral soils, independently of soil composition and texture, up to $\theta_v < 0.5$ cm^3 cm^{-3} (Muñoz-Carpena et al., 2005; Topp et al., 1980). A specific calibration is required for higher water content and organic or volcanic soils.

The relationship between volumetric soil water content (Θ_v) and bulk dielectric constant (ε_b) depends on the electromagnetic wave frequency. It is more soil-specific at low frequencies (<100 MHz) (Muñoz-Carpena et al., 2005). Alternative relationships to the empirical equation (Eq. (1) are the three-phase mixing model (Roth et al., 1990) and the four-phase mixing model (Dobson et al., 1985), which requires dividing soil moisture into mobile and immobile regions (Dirksen and Dasberg, 1993). Mainly, two different PSS techniques rely on the dielectric properties, i.e., time/frequency domain reflectometry and ground penetrating radar.

The dielectric constant is commonly measured by recording the propagation velocity or reflection of an electromagnetic pulse through the soil using probes or antennas in contact with, or placed above, the surface. Time Domain Reflectometry (TDR) and Frequency Domain Reflectometry (FDR) determine ε_b by measuring the travel time or resonant frequency of the signal along a waveguide inserted into the soil, while Ground Penetrating Radar (GPR) estimates ε_b from the two-way travel time of radar waves between the transmitter and receiver. These methods allow non-destructive and in situ measurement of the bulk dielectric constant, which can then be converted into volumetric water content using the empirical or physically based relationships described above.

2.4.1. Time domain reflectometry (TDR)

Time domain reflectometry (TDR) is a technique that was used originally for testing high-speed cables (Ferré and Topp, 2000). TDR was adapted to estimate at the same time both soil water content (Davis and Chudobiak, 1975; Topp et al., 1980) and soil bulk electrical conductivity (Dalton et al., 1984). The water content depends on the polarizability of the water molecules, and the bulk electrical conductivity depends on the attenuation encountered. A waveguide or probe of known length L is embedded in soil, and the travel time (t) for a TDR-generated electromagnetic ramp to cross the probe length is determined. The end of the probe is a point of 'discontinuity' where the electromagnetic signal is reflected. The travel time t allows computing the bulk dielectric constant of soil surrounding the probe as a function of the propagation velocity

$$v = 2L/t \quad (2)$$

$$\text{According to the equation}: \varepsilon_b = \left(\frac{c}{v}\right)^2 = \left(\frac{ct}{2L}\right)^2 \quad (3)$$

where c is the speed of light in vacuum (3×10^8 m s^{-1}), t is the travel time for the pulse to cross the length of the embedded waveguide (2 L: down the soil and back).

The widespread use of TDR has led to several efforts focused on finding alternatives to Eq. (1). A critical review of the models used to determine soil volumetric water content using the bulk dielectric constant measured by TDR is available in He et al. (2023).

A typical TDR instrument consists of a device capable of producing a series of precisely timed electrical pulses with a wide range of high frequencies (e.g., 0.2–3 GHz) traveling along a transmission line constructed with a coaxial cable and a probe (Muñoz-Carpena et al., 2005). There are several different geometrical probe configurations, all of which have a single central conductor and one to six outer conducting rods, consisting of two, three, or six metallic wires and two parallel plates (Jones et al., 2002).

2.4.2. Frequency domain: capacitance and frequency domain reflectometry (FDR)

Frequency domain reflectometry (FRD) is based on the detection of changes in soil water content by changes in the circuit's operating

frequency using a capacitor and an oscillator (Muñoz-Carpena et al., 2005). In the FDR, the oscillator frequency is swept under control within a specific frequency range to find the most significant amplitude. This is known as the resonance frequency and represents a measure of the water content in the soil. Probes consist of two or more electrodes that are inserted into the soil. Electrodes can be metallic plates, rods, or metal rings around a cylinder. In the case of a ring configuration, an access tube is installed in the field in which the probe is introduced. The access tube enables multiple sensors to take measurements at various depths (Muñoz-Carpena et al., 2005).

2.4.3. Ground penetrating radar (GPR)

Ground Penetrating Radar (GPR) operates between 10 MHz and 3 GHz frequency range, within the radio wave region of the EM spectrum (Fig. 6). Like TDR and FDR, GPR primarily responds to subsurface variations in relative dielectric permittivity (RDP), with energy transport dominated by polarization and displacement currents (Everett, 2013b). Electrical conductivity (EC) has a significant influence on signal attenuation during wave propagation (Davis and Annan, 1989). The most common survey configuration is the common-offset reflection mode, where fixed-geometry transmitter and receiver antennas are moved across the surface. Reflected signals from dielectric contrasts are recorded as waveforms (A-scans), which are then assembled into 2D profiles (B-scans) or 3D volumes (C-scans). Depth conversion is possible via velocity calibration using known subsurface targets (such as soil layer boundaries or objects) or hyperbola fitting on round shaped objects in the subsoil.

Despite offering high spatial resolution among near-surface geophysical methods, GPR's application in PSS is constrained by data analysis time, its difficulty in detecting gradual soil texture changes with depth, signal loss due to scattering, absorption, and geometrical spreading (Reynolds, 1997). The method resolution decays with penetration depth due to frequency-dependent attenuation (Bradford, 2007); higher-frequency systems provide finer resolution but have a shallower reach.

GPR is widely used in agricultural contexts for water management (Huisman et al., 2001; Liu et al., 2016), as well as mapping soil layer thickness, stratigraphy, and tree root systems or sometimes drainage pipes (Comas et al., 2015; Zhang et al., 2014). Outside of agricultural applications, GPR is used in archaeology, environmental assessments, road construction analysis, and more. Emerging drone-mounted GPR systems show promise for rapid mapping of root-zone moisture and EC (Wu and Lambot, 2022).

2.5. X-ray fluorescence

X-ray fluorescence (XRF) is a type of spectroscopy that involves the emission of X-ray photons following the excitation of electrons in a sample by primary X-ray photons. When the sample is exposed to X-rays, the atoms within it absorb the photons if their energy is higher than the binding energy of the core–shell electron. When photons are absorbed, they cause the ejection of core–shell or subshell electrons, which are also called photoelectrons. This process leaves behind a vacancy in the core–shell or subshell, putting the atom in an excited state. After absorption, XRF emissions occur when an electron transitions from an upper subshell to fill the electron vacancy, resulting in a de-excitation process that emits a corresponding photon. These emitted XRF photons have unique energies characterizing the electron transition in the given atom, and so the spectroscopic lines can be assigned to specific chemical elements. The intensity of each characteristic energy level is directly proportional to the number of atoms in the respective elements involved in the process, allowing for the measurement of element concentration (Jenkins et al., 1995).

In the 1990 s, the extensive instrumentation used for the XRF process was downsized and made more portable. This led to the creation of modern portable fluorescence instruments, also known as pXRF or handheld XRF. Small, portable instruments with a gun design (Fig. 7) now use a vacuum-sealed tube, approximately the size of a coin, as the source of primary X-ray radiation. The tube has a metal anode (such as Ag, Rh, Ta, Au, W, and others) that is hit by electrons accelerated to 20–60 kV. This collision produces X-rays that correspond to the characteristic K and L line fluorescence of the target atoms, as well as a less intense continuum. The source of emission is situated near the front aperture of the instrument, which comes into contact with the sample. Then, the detector captures the entire emitted spectrum and separates the signals using the energy-dispersive principle (EDXRF) (Beckhoff et al., 2007; Shackley, 2010).

The XRF technique is widely used for determining elemental concentrations in various matrices, including soils. Advancements in pXRF technology and applications are well-documented in annual atomic spectrometry updates (e.g., Potts and Sargent, 2022; Vanhoof et al., 2022). pXRF can function as a qualitative, semi-quantitative, or quantitative analytical tool. The USEPA Method 6200 (2007) offers a comprehensive guide for pXRF use in soil and sediment analysis, highlighting pre-calibration modes (e.g., Geochem, Soil, Mining) provided by manufacturers, and other laboratory-based standards such as EN 15309:2007 that provide protocols XRF spectrometry. It is essential to note that pXRF measures total elemental concentrations, unlike traditional wet methods (e.g., aqua regia extractions as per ISO 11466 or USEPA 3051a), which often yield lower, pseudo-total values, depending

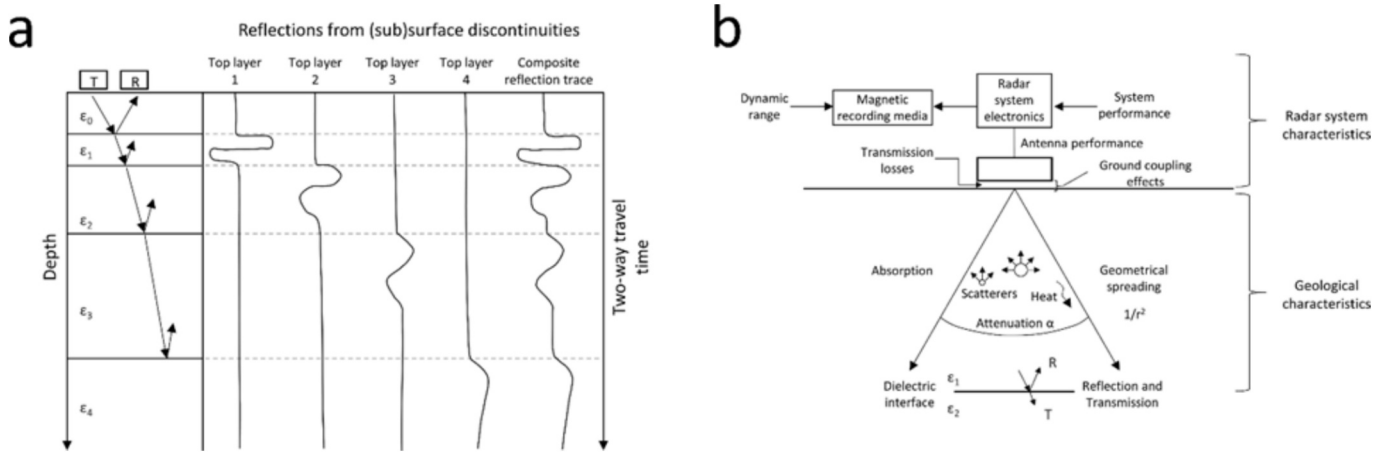

Fig. 6. Schematic diagram showing the working principle of a ground penetrating radar: (a) wave propagation and reflection at the boundaries of media with different relative dielectric permittivity (RDP) and (b) processes that lead to a reduction of signal strength (modified from Conyers (2004); Reynolds (1997)).

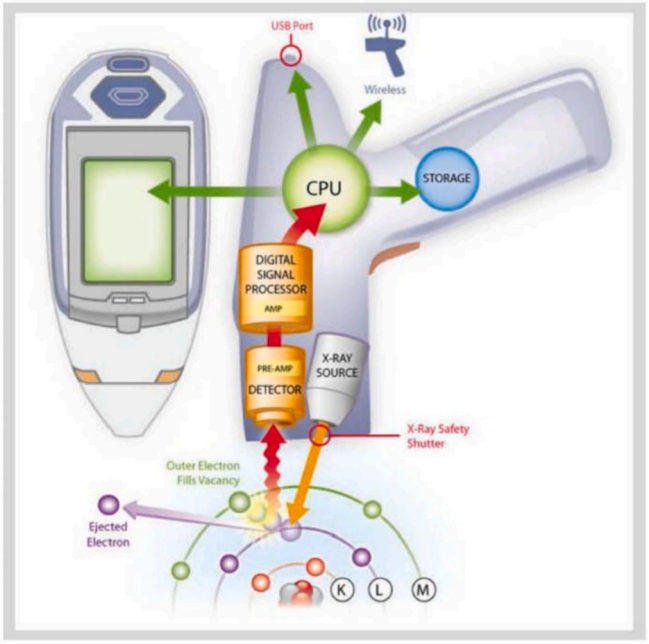

Fig. 7. Schematic design of a portable X-ray fluorescence (pXRF) instrument (with permission of Thermo Fisher, Waltham, MA, USA).

on the element and soil type.

Unlike the other techniques covered in this article, XRF is used directly to determine elemental contents, not requiring proxies to convert spectral readings into elemental content. However, it must indeed use specific algorithms to compensate for the complex spectral interactions that X-rays produce at the atomic level. Beyond the direct determination of elemental concentrations in the soil, the technique has been used to predict from these i) the concentrations of available forms of plant nutrients (Antonangelo and Zhang, 2024; Tavares et al., 2023); ii) other soil properties that are indirectly related to the elemental composition (McBratney et al., 2011b, Tóth et al., 2019) or iii) the concentration of elements (such as C or N) that do not emit an RX signal under the measurement conditions of portable instruments (de Faria et al., 2022; Song et al., 2024).

2.6. Combined techniques

The fusion of measurements obtained from a range of sensors is becoming increasingly common, often improving the prediction of soil properties and chemical elements' concentrations in soil samples (Schmidinger et al., 2024). Independent measurements from functionally different techniques offer a broader insight, providing information on a wide range of soil properties and their spatiotemporal changes. Sensor fusion is a broad term, and as indicated by Ji et al. (2019), there is no consensus on a standard definition. In the case of soil sensors, fusion has been performed by combining data from two or more sensors, using a range of statistical methods, including linear and non-linear regression techniques, as well as more sophisticated approaches such as Granger and Ramanathan's model averaging procedure (1984) and others (Ji et al., 2019). Several authors have suggested using auxiliary soil properties or sensory data in conjunction with Vis-NIR for enhanced soil characterization (Morgan et al., 2009; Brown et al., 2006; Wang et al., 2015). For example, Veum et al. (2015) found that augmenting vis-NIR spectral data with laboratory measurements of pH and bulk density led to improved estimations of soil health indicators related to physical and chemical components. In a subsequent study, vis-NIR was fused with EC and penetration resistance data, resulting in improved estimation of soil health indicators (Veum et al. 2017). In another example, it was noted that for optical sensors like NIR and MIR, the accuracy of indirect property estimations can be improved by incorporating other predictors, such as elemental XRF, which provides contrasting and complementary information (Greenberg et al., 2023). A combination of these two types of sensors was reported in multiple studies for the improvement of SOC, N, P, Mg, Ca, Na, pH, and texture estimations (Javadi et al. 2021; Wang et al. 2013; O'Rourke et al. 2016; Towett et al., 2015; Wang et al., 2015; Weindorf et al., 2016; Tavares et al., 2020; Greenberg et al. 2023). However, no generalizable conclusions can be drawn as the results of fusion were contradictory. As suggested by Greenberg et al. (2023), systematic testing to gain an in-depth understanding of the prediction mechanisms, depending on the property of interest, sensor type, the principle of parsimony, and the method of sensor fusion, is crucial.

In our study, we addressed this issue by analyzing the effect of combining data from two or more proximal sensors, which we refer to as the 'combined techniques.' Additionally, we separately examined the combination of proximal sensor data and traditional laboratory measurements, along with covariates from various sources, including remote sensing and morphometry. In the case of multiple soil sensors being integrated into a single unit, several advantages were listed, including more robust operational performance, increased confidence as different sensors measure the same soil, higher coverage of attributes, and increased dimensionality of the measurement space (Viscarra Rossel et al., 2011). The use of mobile platforms supporting different soil sensors has been reported by several authors, showing the potential for combined on-the-go measurements for improved estimation of physical and chemical soil properties such as pH, EC, bulk density, soil water, SOC, potassium, nitrogen, and other nutrient contents (Lund et al. 2005; Adamchuk and Christenson, 2005; Taylor et al. 2006; Kweon et al., 2008; Yurui et al., 2008; Knadel et al., 2011; Knadel et al., 2015; Tabatabai et al., 2019). Their results demonstrate that multi-sensor systems can be beneficial and practical for conducting field surveys. Yet, customized configurations can be logistically cumbersome and technically challenging to implement synchronously.

3. Methods

In the context of the ProbeField project, bibliographic research was foreseen as the basis for tracking the cost and accuracy of PSS. Literature sources and databases were consulted between October 2022 and December 2023. The resulting set of documents collected from that literature search was used to perform the analyses shown in this work. The process was visually summarized in a schematic workflow (Fig. 8).

3.1. Literature search strategy

All collected papers related to 1) the accuracy of proximal soil sensors and 2) the costs involved in the different steps of soil surveying with PSS were retrieved from search engines such as Scopus and Web of Science.

The keywords used for the review of accuracy of proximal soil sensors were "precision farming," "proximal sensing," "soil sensing," "proximal sensors," "digital soil mapping," "high-resolution mapping," "quasi 3D mapping," "diffuse reflectance spectroscopy," "Vis-NIR," "soil spectroscopy," "gamma-ray spectroscopy," "radiometric," "radionuclides," "X-ray fluorescence," "electromagnetic induction," "georadar," "GPR," "ground penetrating radar," "time-domain reflectometry," "TDR," "data fusion," "combined sensors," "combined techniques," The terms "soil properties estimation," "soil organic carbon," "soil moisture," "clay," "sand," "soil texture," and "nutrients" were used in combination with the keywords listed above to further narrow the spectrum of aimed publications to the PSS context. The keywords for the research on the costs involved in the different steps of soil surveying with PSS were the same as for the accuracy of proximal sensing, with the addition of the keyword "cost" during the literature search strategy (e.g., "soil proximal sensing costs," "diffuse reflectance spectroscopy costs," etc.).

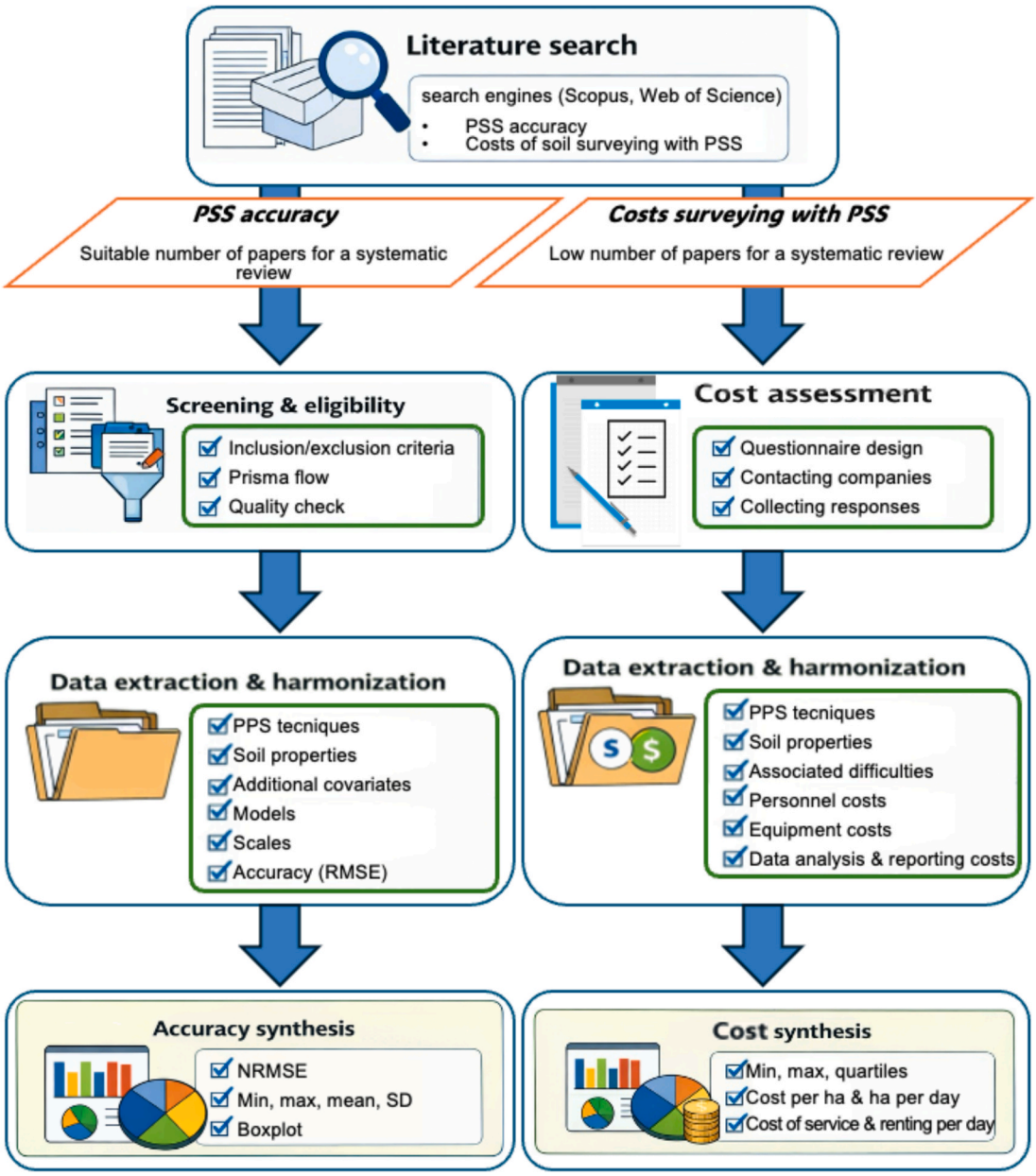

Fig. 8. Schematic workflow of the review process.

The complete list of keywords and strings is shown in Table A1 in the supplementary materials.

Due to the low number of papers resulting from the cost inquiry, a dedicated questionnaire was developed to conduct interviews with commercial companies offering PSS services. Additionally, due to the low number of articles, reports, and papers on cost analysis that align with the objectives of this review retrieved from the bibliography, no exclusion criteria were applied to the collected documents for full-text review.

3.2. Inclusion/exclusion criteria

Original research articles were manually selected, while non-eligible sources, such as non-English studies, extended abstracts, presentations, conference proceedings, reviews, *meta*-analyses, and entire books, were excluded. All articles retrieved for full-text reading were screened by the authors of the present work, each with their own set of designated articles, with the variables of interest collated in a data extraction sheet. Articles included in the analysis should refer to digital soil mapping attempts or to soil property estimation using modelling techniques based on proximal soil sensing covariates. Additionally, papers should report the performance indices of the models employed to estimate the soil properties, as well as the ranges of soil property analytical values determined by wet chemistry. Duplicated papers that did not contribute to the objectives of the review work were manually removed. Articles referring to the use of electromagnetic sensors for digital soil mapping and precision agriculture attempts addressed using UAV platforms or remote sensing alone, PSS techniques that didn't meet the ProbeField's project aims, and efforts on monitoring, reporting, and verification (MRV) systems were excluded from this analysis. Although numerous studies (Fedeli et al., 2024; Horta et al., 2021; Xia et al., 2019) have demonstrated the effectiveness of both laboratory-based and portable X-ray fluorescence (XRF) instruments, studies referring to XRF solely for elemental concentration and mapping were excluded, while focusing instead on those that derived additional properties from portable XRF (pXRF) measurements.

The complete list of papers and associated DOIs used for this analysis is summarized in Table A2 in the supplementary materials, whereas the PRISMA (Page et al., 2021) flowchart with the number of retrieved and excluded documents is also included (Fig. A1). A simplified version of the Mixed Method Appraisal Tool (MMAT) was used to assess quality and the risk of bias in this systematic review. All selected documents met the MMAT criteria for quantitative descriptive studies.

3.3. Literature data extraction and harmonization

An association between the DOIs and the information collected from research papers in the data extraction sheet was performed considering the following qualitative aspects: utilized PSS techniques single or in combination, the sensor employed, the platform type used to perform the survey with the sensor, the soil property or properties investigated, the type of data produced (i.e., both bi-dimensional and tri-dimensional spatializations, and point estimations), any additional covariate used to generate the estimations, the modelling technique, the scale of the study, general characteristics of the study area, soil type, land use, experimental design, and sampling characteristics such as the number of sampling locations, the total number of samples collected per surface unit, and the analytical methods used to measure the soil properties under investigation. A total of 42 soil properties were identified across the entire set of documents, which were subsequently summarized into groups to improve representativeness during data analysis (Table 1).

The collected quantitative information [i.e., normalized RMSE (NRMSE) and analytical values] was entered into a separate sheet to facilitate data analysis, as described below.

Table 1
Summary of soil properties collected from the literature and organized into groups of properties.

Soil property group	SOIL PROPERTIES
Soil carbon (C)	Total carbon (TC)
	Soil organic matter (SOM)
	Soil organic carbon (SOC)
Nitrogen (N)	Total Nitrogen (N)
Nutrients, CEC, and exchangeable bases	Phosphorus (P)
	Potassium (K)
	Cation exchange capacity (CEC)
	Plant available potassium (paK)
	Exchangeable Magnesium (ex-Mg)
	Exchangeable Calcium (ex-Ca)
	Exchangeable Phosphorous (ex-P)
	Exchangeable Potassium (ex-K)
	Other secondary nutrients
Acidic-basic properties	Soil inorganic carbon (SIC)
	Carbonates ($CaCO_3$)
	Salinity (ECe)
	Exchangeable Aluminium (ex-Al)
	Base saturation percentage (BSP)
	Electrical conductivity (EC)
	Lime buffer capacity (LBC)
	pH
	H + Al
Mineralogy	Other chemicals (e.g., potentially toxic elements)
	Clay type
Hydrological properties	Moisture
	Volumetric water content (VWC)
	Field capacity
	Evapotranspiration
	Wilting point
Bulk density (BD)	Bulk density
Soil depth	Soil depth
Texture	Coarse fragments
	Silt, sand, and clay contents
Profile features & other properties	Horizons
	Compacted layer
	Soil structure
	Penetration resistance
	Total porosity
	Biological properties

3.4. Cost survey and questionnaire design

Several questions about the derived cost of applying PSS services in the private sector that aligned with the research topics of the ProbeField project were structured as a questionnaire and translated into four languages (English, German, Spanish, and Italian). The four versions of the questionnaire are available in the supplementary materials of this study. The questionnaire was distributed to PSS companies via the Google Docs platform, along with a letter of introduction to the ProbeField project, or, sometimes, more informally via telephone interviews. It was submitted to numerous PSS companies worldwide, although higher representation was found across Europe, North America, and Midwestern Asia.

The questionnaire is structured as follows: 1) a set of general questions about the activity of the company regarding used sensor types, types of products, and services they offer; 2) a set of specific questions about the use of proximal sensors on-the-go, about what are the critical points referred to the using of sensors, analysis of data, and reporting that have more influence on the final cost such as weighted costs based on personnel costs, working days, equipment costs, etc.; 3) which soil properties are estimated with which sensors, number of samples taken per hectare, the most used line spacing in survey and if equipment is available for rent; 4) specific questions about what are the critical points referred to the traveling to the area of interest, workability, and field characteristics; and 5) two last sets of questions about calibration and validation methods of the final product. In all sections, companies were asked to roughly assess the cost as a percentage range of the total for each step of the process. Finally, a section was proposed for companies to make further comments and suggestions for future research on PSS.

3.5. Data analysis

3.5.1. Accuracy synthesis (descriptive systematic review)

This study follows a systematic review methodology, in accordance with structured literature identification and screening, and provides a descriptive synthesis of reported results. Consequently, this methodology did not match the analytical procedure of a *meta*-analysis. The collected accuracy information was summarized into a single data frame. Each row contained the value of RMSE (Eq. (4) and the minimum and maximum analytical values of the predicted soil property as reported in the respective papers. That quantitative information was associated with the following columns based on the information collected from the retrieved papers (Table 2): A) to the PSS-derived covariate used to model the target property, henceforth, PSS technique (i.e., DRS, EMI/ER, γ-ray, XRF, TDR/FDR, and combined techniques); B) to other variables eventually used besides the sensors' signal response, that were grouped into macro categories such as morphometry, remote sensing, other soil properties, and their combinations. In this work, we refer to such a set of macro categories of variables synthetically as "other covariates" (Table 2); C) to the type of model used to get the estimated soil property, which was classified into the groups "linear" and "non-linear" modeling (Table 2); D) to the group of soil property associated with the accuracy estimation (Table 1); E) to the soil strata where the estimation is performed, that is, topsoil (i.e., 0–30 cm depth) or subsoil (i.e., >30 cm depth); and F) to the scale of the research (i.e., local, non-local). In order to compare the resulting distributions, the following descriptive statistics were calculated: the range from minimum to maximum, the average, the standard deviation, and the 1st and 3rd quartile values, which were reported as charts (i.e., boxplots) or table form. Table 2 provides details about the grouping factors associated to each NRMSE value.

We recall that the following equation gives RMSE:

Table 2
Summary of groups used in the data set for harmonizing the collected accuracy records of using proximal sensors from the literature (techniques, other covariates, and the scale of reference of the study.

Grouping factor	Categories within grouping factors	Description of categories
Techniques	EMI/ER	Electromagnetic induction and electrical resistivity
	γ-ray	Gamma-ray spectroscopy
	GPR	Ground penetrating radar
	XRF	X-ray fluorescence
	DRS	Diffuse reflectance spectroscopy (Vis-NIR-MIR)
	TDR/FDR	Time domain reflectometry and Frequency domain reflectometry
Covariates	Remote sensing	Drone, aerial image, satellite
	Soil property	Wet chemistry, soil class
	Morphometry	Digital elevation model (DEM) and derivatives of DEM (i.e., slope, orientation, hydrography, hydrological basin, etc.)
Scale	Local	Field(s) scale
	Non-local	Includes regional, national, continental scales, together with larger areas (e.g., several sparse fields within a single or more pedoclimatic or administrative zone) not defined by the previous "Local" (field) scale.
Model	Linear (LM)	Generalized linear model (GLM); Spatio-Temporal Generalized Linear Models (SGLM); Linear regression (LR), Stepwise Multiple Linear regression (SMLR); Partial least squares regression (PLSR); Latent variable partial least squares (L-PLS); Ordinary Least Squares regression (OLS); Granger-Ramanathan Combination; K-means(KM); Kriging; Regression kriging; Geographically weighted regression (GWR); Langmuir-Goodwin-Richards (LGR) model; Linear mixed-effects models (LMEm); odds ratio (OR); PCR; quasi-3D modeling
	Non-Linear (NLM)	Machine learning; Machine learning + regression residuals (MLRR); Artificial neural network (ANN); Convolutional neural network (CNN); XGBoost (XGB); Cubist regression (CR); Regression tree (RT); Random Forest (RF); RF and regression residuals (RFRR); Support vector machine (SVM); SVM and regression residuals (SVMRR); PLS–support vector machine (PLS–SVM); Classification and Regression Tree (CART); Multivariate Adaptive Regression Splines (MARS); Penalized Spline Regression (PSR); Generalized additive model (GAM)

$$RMSE = \sqrt{\frac{\sum_{i=1}^{N}(y_i - \hat{y}_i)^2}{N}} \quad (4)$$

where N is the number of data points, y_i is the i^{th} measurement, and $\hat{y}_i$ is its corresponding prediction. In addition, the normalized root-mean-squared error (NRMSE, Eq. (5) was calculated and used alongside the remaining grouping factors, and analytical values for each RMSE record, to make the accuracies comparable across soil properties with variable ranges. The NRMSE was calculated by dividing the RMSE by the range of the soil property, using the following formula:

$$NRMSE = \frac{RMSE}{y_{max} - y_{min}} \quad (5)$$

where y_{max} and y_{min} are the maximum and minimum analytical values of the soil property object of study, RMSE is the metric of accuracy as reported in papers. We decided to normalize by the maximum and minimum values, as this was the most appropriate given the available data. The normalization based on quartiles (e.g., Q_3–Q_1) was also evaluated, as it can reduce the metric's sensitivity to skewed distributions and extreme values, which may otherwise artificially compress the range. However, quartile values are seldom reported in the studies reviewed, making min–max normalization the only consistently applicable approach across the dataset.

3.5.2. Analysis of cost

3.5.2.1. Analysis of costs from literature. After reviewing a selection of papers that included the keyword 'cost' alongside topics such as precision farming and proximal sensing, we skimmed those that enabled us to assess and compare overall budgets. We then refined the list by focusing on studies involving on-the-go or point-based sensors that allow for comprehensive soil characterization. This selection also took into account financial factors, labor hours, and the benefits compared to traditional approaches that do not use proximal sensors, as well as how costs can vary non-linearly depending on the size of the investigation area.

3.5.2.2. Analysis of questionnaire's replies. A semi-quantitative analysis using basic descriptive statistics was conducted on responses to the questionnaires from companies. The non-quantitative replies were summarized based on several factors, including the sensors employed in surveys, the target soil properties, the implementation of fieldwork, and associated difficulties encountered during fieldwork. On the other hand, replies regarding costs were classified into three categories: i) personnel costs, including traveling to the area of interest, ii) equipment costs, and iii) cost of data analysis and reporting. Quantitative data such as costs, areas, and distances were standardized using the qualitative and semi-quantitative information provided by companies as follows: a) costs were reported and transformed to € when necessary; b) areas were converted into hectares (ha), and c) distances to meters (m) for comparison purposes. When the availability of data permitted it, the quantitative information was summarized using descriptive statistics (i.e., the range from minimum to maximum, the median, and the 1st and 3rd quartile values). Due to privacy agreements with companies, this dataset is not being made publicly available. The structure of the questionnaire is available as supplementary material.

4. Results on accuracy

4.1. Dataset description

A total of 1,544 NRMSE records from 114 papers are included in the dataset (Table 3). The resulting dataset is available at the repository ZENODO (https://doi.org/10.5281/zenodo.17121809). DRS is the most frequently used technique individually (32.6 %). Applications for XRF (14.2 %), EMI/ER (11.9 %), γ-ray (8.8 %), and TDR/FDR (2.3 %) are less common. Among applications that utilize combined techniques, which account for 30.1 % of the total, the most investigated combination was EMI/ER + γ-ray (41.4 %). Moderately investigated were the combinations of DRS with XRF and EMI/ER (23.8 % and 15.1 %, respectively). A lower number of applications were found for the following combinations: EMI/ER + γ-ray + DRS, DRS + TDR/FDR, EMI/ER + TDR/FDR, EMI/ER + GPR, γ-ray + XRF (6.8 %, 4.6 %, 1.5 %, 0.9 %, and 0.7 %, respectively).

Based on the number of papers, the most studied groups of soil properties (Table 4) were in order: C (58 %), texture (38.6 %), acidic-basic soil properties (30.7 %), and nutrients, CEC, and exchangeable bases (25.4 %). This last group accounted for the highest number of NRMSE records.

Table 3
Composition of the dataset in terms of techniques. Both the number of papers (i.e., collected DOIs) and the number of observations (Obs.) were reported as raw numbers (n) and as percentages (%). On the left, observation and DOIs are reported for techniques applied individually, whereas on the right, the data zoomed in on the types of combinations that occurred.

Type	Single techniques Observations n	%	DOI n	%	Combined techniques Combination		Observations n	%	DOI n	%
DRS	504	32.6	55	48.2	EMI/ER	γ-ray	192	41.4	11	31.4
XRF	220	14.2	21	18.4	XRF	DRS	139	23.8	10	28.6
EMI/ER	184	11.9	19	16.7	EMI/ER	DRS	48	15.1	8	22.9
γ-ray	136	8.8	11	9.6	EMI/ER	γ-ray + DRS	40	6.8	1	2.9
TDR/FDR	36	2.3	5	4.4	DRS	TDR/FDR	27	4.6	2	5.7
Combined techniques	464	30.1	35	30.7	EMI/ER	TDR/FDR	9	1.5	1	2.9
					EMI/ER	GPR	5	0.9	1	2.9
					γ-ray	XRF	4	0.7	1	2.9
Total	1544	100.0	114	100.0	Total	464	100.0	35	100.0	

DRS: diffuse reflectance spectroscopy; γ-ray: gamma-ray spectroscopy; EMI/ER: electromagnetic induction/electrical resistivity; TDR/FDR: time-domain reflectometry/frequency-domain reflectometry; XRF: X-ray fluorescence; LM: linear modeling; NLM: non-linear modeling.

Table 4
Composition of the dataset in terms of groups of properties. Both the number of papers (i.e., collected DOIs) and the number of observations (Obs.) were reported as raw numbers (n) and as percentages (%).

Groups of properties	Observations n.	%	DOI n	%
Nutrients, CEC, and exchangeable bases	374	24.2	29	25.4
C	347	22.5	67	58.8
Texture	324	21.0	44	38.6
Acidic-basic properties	154	10.0	35	30.7
Hydrological properties	146	9.5	18	15.8
Mineralogy	58	3.8	2	1.8
N	55	3.6	20	17.5
Soil depth	46	3.0	4	3.5
BD	30	1.9	8	7.0
Profile features and other properties	10	0.6	2	1.8
Total	1,544	100.0	114	100.0

CEC: cation exchange capacity, C: carbon, N: nitrogen, BD: bulk density.

4.2. Results for accuracies

Table 5 reports the accuracies filtered by the PSS technique and the group of soil properties. The average NRMSE equals 0.217 for the whole dataset (Table 5). However, when groups of soil properties are considered individually, the overall NRMSE varies mainly depending on the measured soil property and the technique employed. Concerning the soil property groups, the top three overall average accuracies revealed are reached in the profile features and other properties group (NRMSE = 0.105, 10 observations), soil depth (NRMSE = 0.123, 46 observations), and mineralogy (NRMSE = 0.129, 58 observations). In contrast, others, such as the soil carbon group, had the lowest average accuracy, with the highest overall NRMSE of 0.390 (347 observations, Table 4). Notice that such a low average accuracy value attributed to the soil carbon group is due to the NRMSE data collected from Zhang et al. (2020), ranging from 3 to 10 (i.e., outliers, see Table 5), who estimated SOC and other properties in three dimensions, as well as predicted values of soil carbon from non-local calibrations such as SSLs, where NRMSE values ranged from 0.6 to 2 (Guerrero et al., 2016; Guerrero and Lorenzetti, 2021). Excluding those values, the accuracy for the soil carbon group equals 0.098 in 311 observations, which becomes the highest average accuracy for a group of properties. Other groups of properties showing low average accuracy estimations were bulk density (NRMSE = 0.201, 30 observations), texture (NRMSE = 0.196, 324 observations), and hydrological properties (NRMSE = 0.193, 146 observations). The N and nutrients, CEC, and exchangeable bases groups reached average NRMSE values of 0.158 and 0.150, with 55 and 374 observations, respectively. From the point of view of PSS techniques, the highest overall average accuracy was found in XRF (NRMSE = 0.131, 220 observations), followed by DRS (NRMSE = 0.135, 504 observations). The on-the-go PSS techniques, EMI/ER, and γ-ray spectroscopy, yielded average NRMSE values of 0.168 and 0.178, with 184 and 136 observations, respectively. The TDR/FDR technique achieved the lowest overall average accuracy values for single PSS techniques (NRMSE = 0.208, 36 observations). In studies where techniques are used in combination in multi-sensor assets (combined techniques group), the NRMSE showed the highest overall average value; in other words, the lowest average accuracy (NRMSE = 0.378, 464 observations). Notice that such low accuracy values are attributed to the sorting of data. As we state later, specific combinations of sensors can be as accurate as single techniques or even higher. The spread of the NRMSE distributions (Fig. 9) varied considerably among techniques. XRF showed the lowest variability, with narrow distributions and few outliers, as indicated by its low standard deviations, whereas DRS and combined sensor approaches exhibited much wider spreads and several extreme values. This greater dispersion is reflected in their higher standard deviations (Table 5).

The DRS technique showed the highest average accuracy in estimating acidic-basic properties (NRMSE = 0.116, 56 observations), nitrogen (NRMSE = 0.125, 27 observations), hydrological properties (NRMSE = 0.020, 2 observations), nutrients, CEC, and exchangeable bases (NRMSE = 0.087, 78 observations), as shown in Fig. 9. Moreover, it was the only PSS technique that provided estimations for the profile features and other properties group (see the paragraph above). XRF showed the highest average accuracy in estimating properties of the mineralogy group (NRMSE = 0.103, 18 observations) and the soil texture group (NRMSE = 0.107, 24 observations). Additionally, XRF demonstrated the highest accuracy in estimating BD (NRMSE = 0.141), although only one observation was found. Amongst the on-the-go PSS techniques, γ-ray spectroscopy achieved the highest average accuracy in estimating soil carbon group properties (NRMSE = 0.116, 5 observations), closely followed by the combined techniques group (NRMSE = 0.169, 85 observations). The EMI/ER technique demonstrated higher average accuracy in producing maps of soil depth (NRMSE = 0.121, 44 observations) compared to γ-ray spectroscopy (NRMSE = 0.174, 2 observations). The combined techniques group never showed the highest average accuracy value among all the groups of properties (Table 5). Instead, it occupied second place in estimating bulk density (NRMSE = 0.174, based on 17 observations) and mineralogy (NRMSE = 0.113, based on 18 observations). Combinations of techniques were also common in estimating other groups of properties, such as acidic-basic properties, nitrogen, hydrological properties, soil texture, and the nutrient, CEC, and exchangeable bases group. Still, they showed generally lower average accuracy compared to the application of single PSS techniques.

Table 6 presents the accuracy of estimations based on the average NRMSE for the group of combined techniques. The combination of DRS and XRF reached higher accuracy values to predict acidic and basic

Table 5
Descriptive statistics of NRMSE grouped by technique and group of soil properties.

Technique	Group of soil properties	Obs.	Min.	Avg.	SD	Max.
DRS		504	0.001	0.135	0.227	3.450
	Acidic-basic properties	56	0.018	0.116	0.068	0.358
	Bulk density (BD)	4	0.102	0.204	0.168	0.455
	C	222	0.003	0.140	0.319	3.450
	Hydrological properties	2	0.001	0.021	0.029	0.041
	Mineralogy	22	0.082	0.165	0.033	0.254
	N	27	0.002	0.125	0.093	0.375
	Nutrients, CEC, exchangeable bases	78	0.035	0.087	0.035	0.178
	Profile features and other properties	10	0.017	0.105	0.039	0.160
	Texture	83	0.032	0.178	0.171	0.723
EMI/ER		184	0.007	0.178	0.131	0.800
	Acidic-basic properties	31	0.007	0.159	0.177	0.731
	Bulk density (BD)	6	0.152	0.262	0.107	0.433
	C	13	0.028	0.132	0.082	0.371
	Hydrological properties	38	0.083	0.234	0.134	0.800
	N	2	0.118	0.152	0.048	0.186
	Nutrients, CEC, exchangeable bases	23	0.066	0.234	0.172	0.661
	Soil depth	44	0.054	0.121	0.036	0.199
	Texture	27	0.026	0.167	0.101	0.343
γ-ray		136	0.010	0.169	0.127	0.726
	Acidic-basic properties	9	0.010	0.123	0.083	0.228
	Bulk density (BD)	2	0.150	0.275	0.177	0.400
	C	5	0.063	0.116	0.057	0.187
	Hydrological properties	3	0.165	0.282	0.177	0.485
	N	2	0.200	0.220	0.028	0.240
	Nutrients, CEC, exchangeable bases	21	0.055	0.225	0.199	0.726
	Soil depth	2	0.159	0.174	0.020	0.188
	Texture	92	0.017	0.156	0.106	0.667
TDR/FDR		36	0.020	0.208	0.231	1.000
	Hydrological properties	36	0.020	0.208	0.231	1.000
XRF		220	0.001	0.131	0.068	0.522
	Acidic-basic properties	24	0.106	0.146	0.027	0.195
	Bulk density (BD)	1	0.142	–	–	0.142
	C	22	0.050	0.123	0.049	0.289
	Hydrological properties	2	0.189	0.206	0.024	0.223
	Mineralogy	18	0.090	0.104	0.012	0.136
	N	18	0.062	0.154	0.064	0.258
	Nutrients, CEC, exchangeable bases	111	0.000	0.134	0.085	0.522
	Texture	24	0.060	0.107	0.028	0.163
Combined techniques		464	0.002	0.378	1.093	10.4
	Acidic-basic properties	34	0.012	0.209	0.168	1.000
	Bulk density (BD)	17	0.069	0.174	0.122	0.455
	C	85	0.002	0.169	2.354	10.358
	Hydrological properties	65	0.025	0.161	0.127	1.000
	Mineralogy	18	0.085	0.113	0.015	0.137
	N	6	0.043	0.303	0.364	1.000
	Nutrients, CEC, exchangeable bases	141	0.038	0.172	0.165	1.000
	Texture	98	0.026	0.280	0.392	2.520
Total		1544	0.074	0.217	0.626	0.791

Where values in the "Total" row represent, respectively, the sum of observations, and the average of values in the successive columns (i.e., the average of minimums, the mean NRMSE of the dataset, the average SD, and the average of maximums).
DRS: diffuse reflectance spectroscopy; γ-ray: gamma-ray spectroscopy; EMI/ER: electromagnetic induction/electrical resistivity; TDR/FDR: time-domain reflectometry/frequency-domain reflectometry; XRF: X-ray fluorescence; LM: linear modeling; NLM: non-linear modeling. CEC: cation exchange capacity, C: carbon, N: nitrogen, BD: bulk density.

properties (NRMSE = 0.157, 13 observations), soil carbon (NRMSE = 0.044, 29 observations), mineralogy (NRMSE = 0.113, 18 observations), nitrogen (NRMSE = 0.142, 3 observations), and nutrients, CEC, and exchangeable bases (NRMSE = 0.084, 62 observations); whereas DRS and TDR/FDR was the combination reaching higher average accuracy to estimate bulk density (NRMSE = 0.098, 9 observations) and hydrological properties (NRMSE = 0.050, 18 observations). The combination of DRS and EMI/ER techniques yielded average NRMSE values of 0.184 in 17 observations in estimating soil texture.

Fig. 10 compares the performance of the best combinations based on the average NRMSE with the average accuracy of predictions achieved using single techniques. This chart illustrates that a specific combination of techniques may yield more accurate predictions compared to the average NRMSE of a single PSS technique. This affects, for example, bulk density, soil carbon, hydrological properties, and the group of nutrients, CEC, and exchangeable bases. In fact, DRS + TDR/FDR for BD and hydrological properties, as well as DRS + XRF for C, and the group of nutrients, CEC, and exchangeable bases, yielded more accurate estimations of those groups.

Table 7 presents the accuracy of spatializations (i.e., thematic maps of soil properties) realized with on-the-go techniques (i.e., EMI/ER, γ-ray spectroscopy, and combined techniques including on-the-go DRS, which was considered as a combination of techniques because it was always employed in multisensor assets in the set of the literature that was checked for this study) in the top and subsoil, respectively. The accuracy of the estimations was assessed by considering the groups of properties. The total number of observations by technique was 171 for EMI/ER (40 topsoil and 131 subsoil), 131 for γ-ray spectroscopy (87 topsoil and 44 subsoil), and 361 for combined techniques (182 topsoil and 179 subsoil). The average NRMSE for EMI/ER in the topsoil was 0.219, and 0.178 in the subsoil. For γ-ray spectroscopy, average NRMSE values of 0.158 were achieved in the topsoil and 0.235 in the subsoil. In the case of combined techniques, the topsoil attained a value of 0.156, while the subsoil achieved a value of 0.279. The ranking of spatializations of groups of properties, from the most accurate to the less precise, was sorted as follows: hydrological properties using combined techniques in the topsoil (NRMSE = 0.086, 24 observations), soil texture fractions with the EMI/ER technique in the subsoil (NRMSE = 0.109, 15 observations), acidic and basic properties using γ-ray spectroscopy in the subsoil (NRMSE = 0.123, 9 observations), nutrient, CEC, and exchangeable bases using γ-ray spectroscopy (NRMSE = 0.132, 2 observations), BD using EMI/ER in the topsoil (NRMSE = 0.153, 2 observations), and finally, hydrological properties in the subsoil with combined techniques (NRMSE = 0.204, 41 observations).

4.3. *Effect of covariates on soil property estimations*

Table 8 shows the NRMSE data organized into sets of studies applying covariates during the modeling process. When the overall average NRMSE of the covariates datasets was compared, higher overall average accuracies were reached when using remote sensing covariates (average NRMSE = 0.116, 24 observations), followed by the average NRMSE value of the dataset in which several covariates are used together (average NRMSE = 0.180, 100 observations), soil properties covariates (average NRMSE = 0.195, 188 observations), and morphometrical covariates (average NRMSE = 0.710, 177 observations). A higher number of observations was found in studies applying combined techniques and morphometrical covariates, where the lowest average accuracy of the whole dataset was observed when estimating the soil carbon group (NRMSE = 2.923, 32 observations). Instead, the most accurate NRMSE average value was obtained when applying γ-ray spectroscopy for estimating soil texture using morphometrical

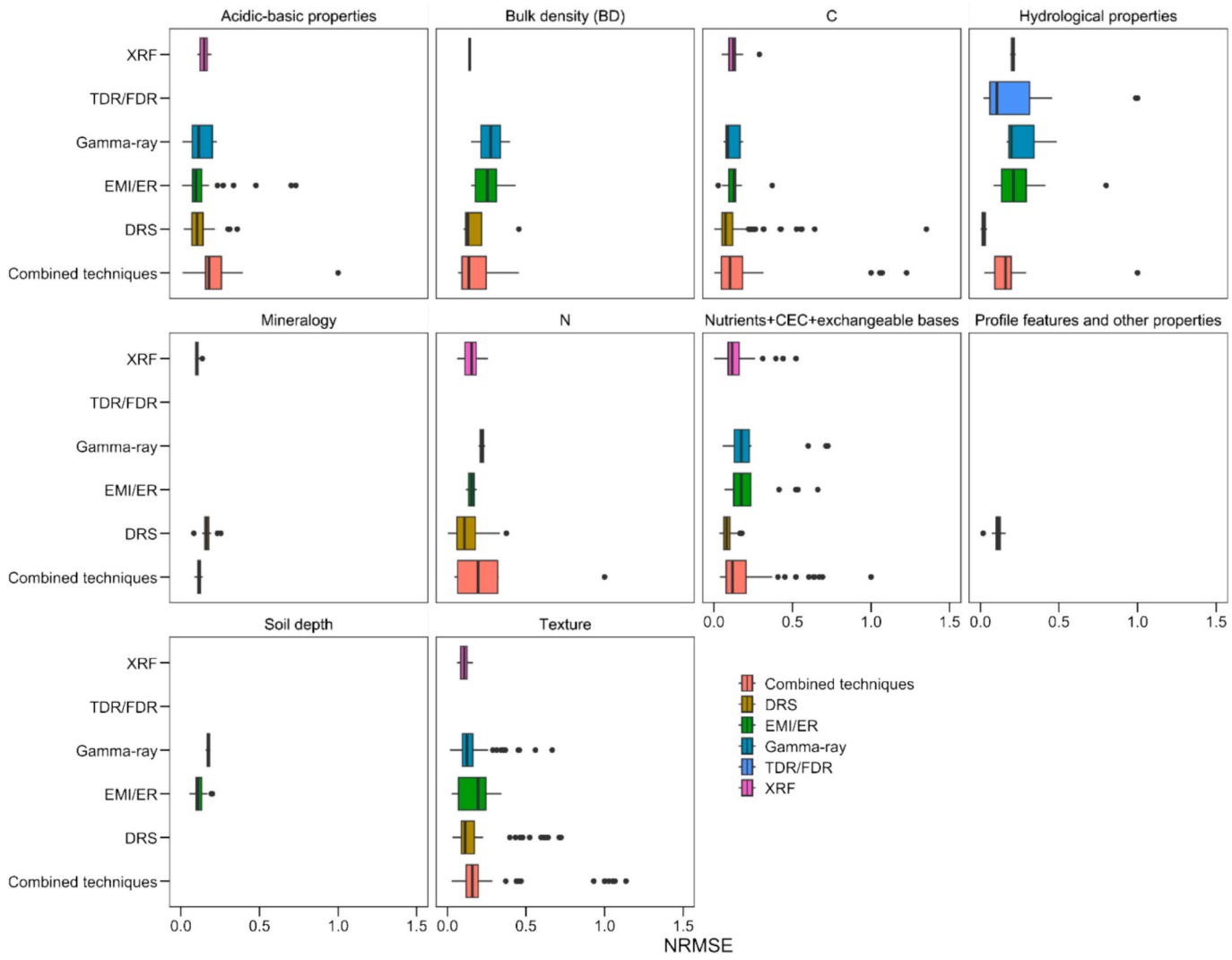

Fig. 9. Diagrams accounting for the normalized root-mean-square error (NRMSE) of each PSS technique estimating the groups of soil properties. NRMSE values over 1.5 are excluded from this chart. DRS: diffuse reflectance spectroscopy; γ-ray: gamma-ray spectroscopy; EMI/ER: electromagnetic induction/electrical resistivity; TDR/FDR: time-domain reflectometry/frequency-domain reflectometry; XRF: X-ray fluorescence; LM: linear modeling; NLM: non-linear modeling. CEC: cation exchange capacity, C: carbon, N: nitrogen, BD: bulk density.

covariates (NRMSE = 0.043). When soil properties are used as covariates, the most frequent technique is XRF (75 observations). Still, the most accurate estimation was found when using the EMI/ER technique for modeling soil depth (NRMSE = 0.100). High average accuracies were obtained when combining DRS with remote sensing covariates to estimate soil carbon (NRMSE = 0.075, 13 observations). It is worth mentioning that the use of several covariates together yielded accurate estimations in combination with XRF soil carbon, nitrogen, and soil texture (NRMSE = 0.083, 0.074, and 0.099, respectively). In addition, the use of more than one type of covariate and combined techniques also yielded accurate estimations (Table 8, see Section 4.5 for details).

4.4. *Effect of the modeling technique on the accuracy of estimations*

Fig. 11 presents the accuracy of the linear modeling (LM) and non-linear modeling (NLM) models filtered by the PSS technique and the group of soil properties. NLM achieved a lower accuracy (average NRMSE = 0.303) compared to LM (average NRMSE = 0.185). However, the accuracy of NLM was found to be superior to that of LM in specific cases. For point-based estimations, NLM outperforms LM: DRS achieved an average accuracy of 0.128, using 85 observations with NLM, compared to an NRMSE of 0.136, using 419 observations with LM. Similarly, XRF estimations with NLM yielded 0.125, 103 observations, and NRMSE = 0.136, 117 observations applying LM. In contrast, the average accuracy of using LM in the specific case of mapping soil properties with EMI/ER exceeds mapping studies using the same technique and NLM (i.e., NRMSE = 0.162, 147 observations vs. NRMSE = 0.240, 37 observations, respectively). Similarly, the average accuracy of using LM to produce maps of soil properties using γ-ray spectroscopy also exceeds that of NLM (i.e., NRMSE = 0.161, 107 observations vs. NRMSE = 0.196, 29 observations, respectively). We did not find studies that utilized NLM for estimating hydrological properties with TDR/FDR in our dataset. Additionally, no NLM applications were found for the specific cases of EMI/ER and γ-ray spectroscopy when estimating acidic and basic properties, bulk density, and nitrogen. The combination of techniques seems to yield better estimations when using LM compared to NLM (NRMSE = 0.290, 292 observations vs. NRMSE = 0.527, 172 observations, respectively). Notice the narrow difference in the comparison between LM and NLM in the accuracy of predictions when point-based techniques are used, and in the case of the accuracy of soil maps, where that difference is significantly wider.

Table 6
Best combinations of techniques for each soil property, according to the mean values of NRMSE. The combinations with an occurrence lower than five are excluded.

Groups of properties	BEST technique combination	NRMSE				
		Obs.	Min.	Avg.	SD	Max.
Acidic-basic properties	DRS + XRF	13	0.024	0.157	0.046	0.222
BD	DRS + TDR/FDR	9	0.069	0.098	0.026	0.141
C	DRS + XRF	29	0.002	0.044	0.049	0.122
Hydrological properties	DRS + TDR/FDR	18	0.025	0.050	0.021	0.108
Mineralogy	DRS + XRF	18	0.085	0.113	0.015	0.137
N	DRS + XRF	3	0.043	0.142	0.158	0.325
Nutrients, CEC, exchangeable bases	DRS + XRF	62	0.038	0.084	0.025	0.136
Texture	DRS + EMI/ER	17	0.026	0.184	0.133	0.468

DRS: diffuse reflectance spectroscopy; γ-ray: gamma-ray spectroscopy; EMI/ER: electromagnetic induction/electrical resistivity; TDR/FDR: time-domain reflectometry/frequency-domain reflectometry; XRF: X-ray fluorescence; LM: linear modeling; NLM: non-linear modeling. CEC: cation exchange capacity, C: carbon, N: nitrogen, BD: bulk density.

4.5. Best combination of factors for soil property prediction

This section displays the mix of factors considered in this systematic review (i.e., PSS technique, covariate, and modeling method) that yields the most accurate estimations of soil properties. Table 9 reports on the top three combinations that achieved the highest accuracy (i.e., lowest NRMSE). The combination "DRS-NLM-no covariates" achieved the best solution for estimating soil properties, including acidic-basic properties, C, mineralogy, and the group of nutrients, CEC, and exchangeable bases. Similarly, the combination "EMI/ER-LM-no covariates" resulted in the best solution for estimating BD, soil depth, hydrological properties, and C. These two were the most common combinations among the whole set of best combinations. Optimal NRMSE scores were also obtained with the combinations: i) DRS-LM-covariates for estimating the acidic-basic group of properties; ii) DRS-LM-no covariates for estimating the group of nutrients, CEC, and exchangeable bases; iii) DRS-NLM-no covariates for estimating the soil carbon group, and nutrients, CEC, and exchangeable bases; iv) XRF-LM/NLM-no covariates to estimate soil texture; v) combined techniques (specifically, DRS + TDR/FDR)-LM-covariates to estimate BD.

5. Results on costs

5.1. Cost data from the literature review

Table 10 summarizes the costs derived from surveys with PSS. Chatterjee et al. (2021) estimated the cost of a PSS survey for predicting

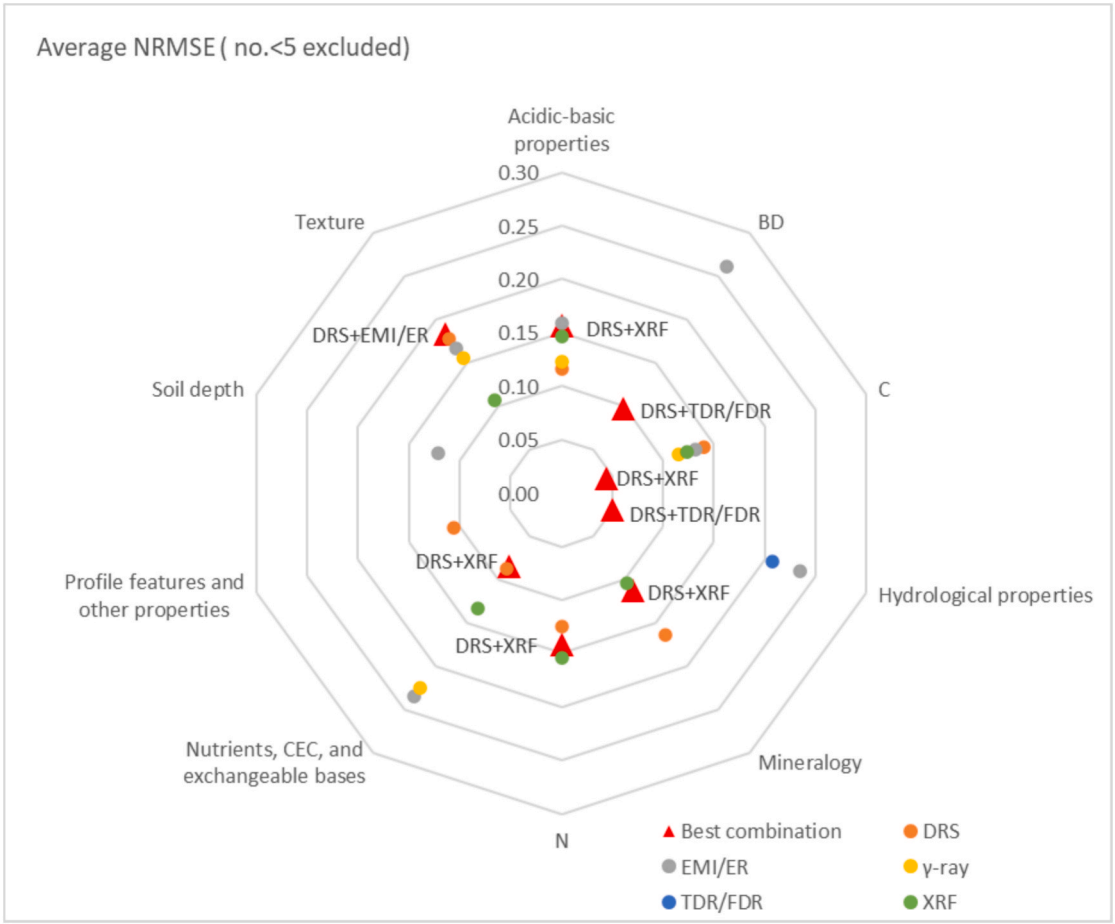

Fig. 10. Radar plot showing the accuracy (NRMSE) of the combined techniques compared with the single technique for each group. The average NRMSE based on a sample size of fewer than five is not included. DRS: diffuse reflectance spectroscopy; γ-ray: gamma-ray spectroscopy; EMI/ER: electromagnetic induction/electrical resistivity; TDR/FDR: time-domain reflectometry/frequency-domain reflectometry; XRF: X-ray fluorescence; LM: linear modeling; NLM: non-linear modeling. CEC: cation exchange capacity, C: carbon, N: nitrogen, BD: bulk density

Table 7
Average and standard deviation of NRMSE, and number of observations for spatializations of each group of properties (maps of soil properties) in the top and subsoil. Combined techniques include combinations of EMI/ER and γ-ray spectroscopy, as well as on-the-go Vis-NIR spectroscopy, which was considered in this category because it was always employed in multisensory assets to produce maps of soil properties.

Soil property group	Layer	Technique								
		EMI/ER			γ-ray			Combined techniques		
		Obs.	Avg.	SD	Obs.	Avg.	SD	Obs.	Avg.	SD
Acidic-basic properties	Topsoil	2	0.244	0.149	–	–	–	21	0.196	0.073
	Subsoil	29	0.153	0.098	9	0.123	0.070	13	0.231	0.171
BD	Topsoil	2	0.153	0.040	1	0.150	0.039	10	0.103	0.044
	Subsoil	4	0.316	0.124	1	0.400	0.104	7	0.275	0.133
Hydrological properties	Topsoil	19	0.276	0.126	1	0.196	0.051	24	0.086	0.055
	Subsoil	19	0.194	0.112	2	0.325	0.144	41	0.204	0.087
N	Topsoil	1	0.185	0.048		–	–	3	0.230	0.095
	Subsoil	1	0.118	0.030	2	0.220	0.064	3	0.375	0.329
Nutrient, CEC, and ex. Bases	Topsoil	4	0.218	0.107	2	0.132	0.036	101	0.129	0.077
	Subsoil	19	0.238	0.169	19	0.235	0.145	40	0.282	0.170
Soil depth	Subsoil	44	0.121	0.049	2	0.174	0.050	–	–	–
Soil texture	Topsoil	12	0.239	0.078	83	0.155	0.085	23	0.193	0.140
	Subsoil	15	0.109	0.076	9	0.171	0.087	75	0.306	0.207
Mineralogy	Topsoil	–	–	–	–	–	–	18	0.113	0.035

DRS: diffuse reflectance spectroscopy; γ-ray: gamma-ray spectroscopy; EMI/ER: electromagnetic induction/electrical resistivity; TDR/FDR: time-domain reflectometry/frequency-domain reflectometry; XRF: X-ray fluorescence; LM: linear modeling; NLM: non-linear modeling. CEC: cation exchange capacity, C: carbon, N: nitrogen, BD: bulk density.

Table 8
Number of observations, averages ± standard deviations of accuracies for groups of soil properties estimation using the other covariates such as morphometrical (i.e., DEM, and derivatives of DEM), soil properties (i.e., SOC, clay, etc.), remote sensing derivatives (i.e., spectral indices, single bands, etc.), and several covariates together.

Groups of	Group of soil	XRF			γ-ray			EMI/ER			DRS			Combined techniques		
Covariates	properties	Obs.	Avg.	SD	Obs.	Avg.	SD	Obs.	Avg.	SD	Obs.	Avg.	SD	Obs.	Avg.	SD
Morphometry derivatives	Acidic-basic properties	3	0.156	0.048	–	–	–	1	0.094	–	15	0.080	0.059	–	–	–
	BD	–	–	–	–	–	–	–	–	–	3	0.055	0.021	–	–	–
	C	–	–	–	–	–	–	1	0.111	–	–	–	–	32	2.923	3.457
	Hydrological properties	–	–	–	–	–	–	1	0.369	–	–	–	–	27	0.185	0.099
	N	3	0.099	0.043	–	–	–	1	0.186	–	–	–	–	–	–	–
	Nutrient, CEC, and ex. Bases	–	–	–	–	–	–	1	0.148	–	–	–	–	4	0.123	0.068
	Soil depth	–	–	–	1	0.159	–	24	0.106	0.046	–	–	–	–	–	–
	Soil texture	6	0.125	0.066	1	0.043	–	6	0.185	0.139	9	0.557	0.267	38	0.368	0.084
Soil properties	Acidic-basic properties	–	–	–	–	–	–	–	–	–	1	0.097	0.025	8	0.321	0.129
	BD	–	–	–	–	–	–	–	–	–	–	–	–	7	0.141	0.055
	C	13	0.133	0.055	–	–	–	2	0.274	0.155	19	0.194	0.097	6	0.271	0.192
	Hydrological properties	–	–	–	–	–	–	–	–	–	–	–	–	11	0.134	0.019
	N	12	0.189	0.130	–	–	–	–	–	–	1	0.142	0.037	1	1.000	–
	Nutrient, CEC, and ex. Bases	48	0.153	0.099	–	–	–	–	–	–	2	0.127	0.041	4	0.544	0.930
	Soil depth	–	–	–	–	–	–	1	0.100	–	–	–	–	–	–	–
	Soil texture	2	0.137	0.048	–	–	–	6	0.234	0.147	10	0.113	0.076	12	0.393	0.488
Remote sensing derivatives	Acidic-basic properties	–	–	–	–	–	–	–	–	–	–	–	–	1	0.229	–
	C	–	–	–	–	–	–	–	–	–	13	0.075	0.038	4	0.121	0.081
	Hydrological properties	–	–	–	–	–	–	–	–	–	–	–	–	1	0.236	–
	Nutrient, CEC, and ex. Bases	–	–	–	–	–	–	–	–	–	–	–	–	2	0.255	0.199
	Soil texture	–	–	–	–	–	–	–	–	–	1	0.119	–	2	0.111	0.038
Several covariates together	Acidic-basic properties	1	0.146	–	–	–	–	–	–	–	–	–	–	5	0.259	0.131
	C	1	0.083	–	–	–	–	–	–	–	–	–	–	20	0.059	0.023
	Hydrological properties	–	–	–	–	–	–	21	0.292	0.185	–	–	–	13	0.174	0.061
	N	1	0.074	–	–	–	–	–	–	–	–	–	–	–	–	–
	Nutrient, CEC, and ex. Bases	–	–	–	–	–	–	–	–	–	–	–	–	30	0.203	0.163
	Soil texture	3	0.099	0.047	1	0.045	–	–	–	–	–	–	–	4	0.126	0.077

DRS: diffuse reflectance spectroscopy; γ-ray: gamma-ray spectroscopy; EMI/ER: electromagnetic induction/electrical resistivity; TDR/FDR: time-domain reflectometry/frequency-domain reflectometry; XRF: X-ray fluorescence; LM: linear modeling; NLM: non-linear modeling. CEC: cation exchange capacity, C: carbon, N: nitrogen, BD: bulk density.

multiple soil properties for an 80-hectare field using combined techniques (XRF and EMI), acquisition of DEM by using LiDAR, acquisition of remote sensing imagery, the analysis of soil samples, and hiring personnel for predicting multiple soil properties at 12.000 $. Priori et al. (2019) estimated costs ranging from approximately 300 € per hectare for small areas (10–30 ha) to about 100 € per hectare for areas larger than 500 ha. Malone et al. (2022) reported a unit cost of approximately 640 $ per hectare for PSS surveys, considering soil core scanning, soil sampling, and sample analysis. Van Egmond et al. (2018) reported that the cost calibration per hectare of soil texture using γ-ray spectroscopy,

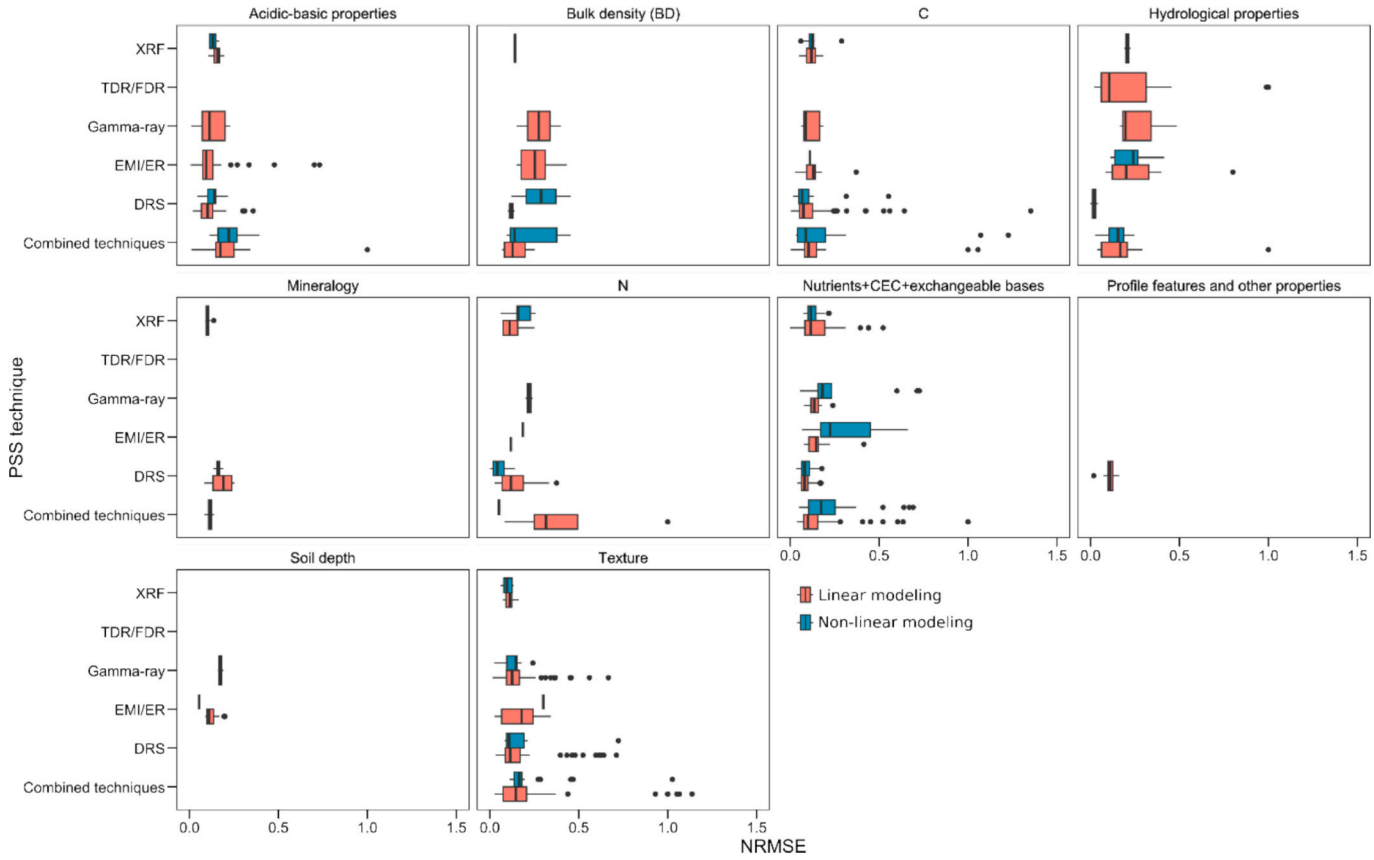

Fig. 11. Effect of applying linear modeling techniques (e.g., multiple regression, partial-least square regression) and non-linear modeling techniques (e.g., random forest, regression trees, support vector machine) on the accuracy (NRMSE) of PSS techniques estimating groups of soil properties. NRMSE values over 1.5 are excluded from this chart. DRS: diffuse reflectance spectroscopy; γ-ray: gamma-ray spectroscopy; EMI/ER: electromagnetic induction/electrical resistivity; TDR/FDR: time-domain reflectometry/frequency-domain reflectometry; XRF: X-ray fluorescence; LM: linear modeling; NLM: non-linear modeling. CEC: cation exchange capacity, C: carbon, N: nitrogen, BD: bulk density.

including soil analysis, ranges from 60 to 67 € when conducted with UAV or car-borne platforms, while the cost reaches 77 € when performed on foot.

5.2. Cost data from the companies' survey

The analysis of questionnaires provided insights into the costs associated with PSS surveys carried out by private sector companies. Out of the 90 companies contacted, only 24 responded. Most of the replying companies operate mainly in the European Union, although companies from North America and Western Asia also provided information. Due to the sensitive nature of cost information, responses varied significantly. Nevertheless, we summarized descriptive statistics of quantitative data extracted from questions related to in-field and service costs (Table 11).

Companies reported covering a range of one to 300 ha per day using on-the-go sensors. The minimum daily coverage was four ha achieved on foot using γ-ray spectrometers and EMI sensors (individually or combined). The maximum coverage was 300 ha using a car platform for γ-ray spectroscopy surveys. The median daily coverage was about 30 ha. Generally, the results show that the wider the covered area is, the lower the cost per hectare. The median cost of a surveyed hectare varies around 142 €, with a minimum of 100 € when car or quad platforms are employed. Notwithstanding, surveys with more than one sensor or highly specialized robotic instruments with multiple sensors can reach very high costs both daily and per hectare (Table 11). The average cost for a PSS service per day oscillated from 2,575 € (Q_1) to 7,025 € (Q_3), while the daily average cost of renting sensors varied from 300 € to 600 €. The main product provided by all companies was soil maps. Only a few companies offered soil sample scanning using spectroscopy, such as vis-NIR or MIR spectroscopy, to track chemical properties such as soil organic carbon (SOC), pH, and nutrients. None of the responding companies offered a characterization of soil samples using XRF. Most companies identified texture, water content, salinity, and nutrients as the most important properties to measure for PA purposes due to their impact on water and fertilization management. The most requested service was soil texture mapping with EMI and γ-ray spectrometers, followed by SOC using vis-NIR spectroscopy. Only three companies reported providing GPR surveys, and one of these applied this technique for geo-engineering services rather than PA. The number of soil samples for soil map calibration and validation varies widely among companies. Some companies reported no soil sampling and claimed to use covariates such as the digital elevation model (DEM) and its derivatives, geological maps, satellite imagery, coring, and information provided by farmers to validate the predictions of soil properties. Most companies collect at least one sample every 2–4 ha. In particular, five out of eight companies used less than 1 sample per hectare (0.2–0.5), two companies reported taking four samples per hectare, and one company claimed to take ten samples. Some companies declared that they base their sampling on the extension of geomorphological units. Additionally, according to the questionnaires, the cost of soil sample analysis varies significantly by region, ranging from 60 to 250 € per sample. In contrast, the GLOSOLAN Standard Operating Procedures (SOPs) established a cost range from 30 to 80 € per sample for a complete standard soil analysis.

Looking at specifics, the cost of PSS is primarily driven by personnel costs (e.g., fieldwork, logistics, and travel to the area of interest), followed by data analysis (including communication), and equipment costs

Table 9
Top-three combination of factors showing the most accurate estimations for each group of soil properties based on the NRMSE.

Groups of properties	Best combination of factors			Type of estimation	Records	NRMSE			
	PSS technique	Model technique	Use of covariates		n.	Min	Mean	SD	Max
Acidic-basic properties	DRS	LM	Yes	Point	16	0.038	0.081	0.025	0.117
	γ-ray	LM	No	Map	9	0.01	0.123	0.083	0.228
	DRS	NLM	No	Point	9	0.043	0.128	0.051	0.216
BD	Combined techniques	LM	Yes	Point/Map	7	0.069	0.095	0.027	0.139
	EMI/ER	LM	No	Map	6	0.152	0.262	0.107	0.433
C	DRS	NLM	No	Point	26	0.014	0.092	0.1	0.553
	EMI/ER	LM	No	Map	10	0.028	0.105	0.04	0.147
	Combined techniques	LM	No	Point/Map	17	0.002	0.11	0.043	0.188
Hydrological properties	Combined techniques	NLM	No	Point/Map	8	0.025	0.052	0.031	0.108
	TDR/FDR	LM	Yes	Point	22	0.02	0.145	0.107	0.359
	EMI/ER	LM	No	Map	12	0.083	0.161	0.072	0.32
Mineralogy	XRF	NLM	No	Point	18	0.09	0.104	0.012	0.136
	Combined techniques	NLM	No	Point/Map	18	0.085	0.113	0.015	0.137
	DRS	NLM	No	Point	18	0.135	0.161	0.014	0.191
N	XRF	LM	Yes	Point	7	0.074	0.134	0.062	0.25
	DRS	LM	No	Point	23	0.026	0.136	0.093	0.375
	XRF	NLM	Yes	Point	9	0.141	0.189	0.048	0.258
Nutrient, CEC, and ex. bases	DRS	LM	No	Point	65	0.041	0.085	0.033	0.173
	DRS	NLM	No	Point	11	0.035	0.089	0.047	0.178
	XRF	LM	No	Point	42	0	0.116	0.09	0.44
Profile features and other properties	DRS	LM	No	Point	10	0.017	0.105	0.039	0.160
Soil depth	EMI/ER	LM	No	Map	12	0.099	0.121	0.023	0.168
	EMI/ER	LM	Yes	Map	31	0.089	0.123	0.039	0.199
Texture	XRF	LM	No	Point	5	0.074	0.093	0.018	0.113
	XRF	NLM	No	Point	8	0.06	0.098	0.03	0.134
	XRF	LM	Yes	Point	11	0.075	0.12	0.028	0.163

DRS: diffuse reflectance spectroscopy; γ-ray: gamma-ray spectroscopy; EMI/ER: electromagnetic induction/electrical resistivity; TDR/FDR: time-domain reflectometry/frequency-domain reflectometry; XRF: X-ray fluorescence; LM: linear modeling; NLM: non-linear modeling. CEC: cation exchange capacity, C: carbon, N: nitrogen, BD: bulk density.

Table 10
Cost breakdown and main parameters for defining budgets for precision mapping activities. Costs are converted into euros for comparison.

Scenario	Fieldwork	Processing	Modeling	Total (€)	Cost/ha (€)	Area (ha)	Sampling locations	N samples	Sample density	Invested time (h)	Reference
EMI + DRS + XRF	470	18,170	270	19,950	250	80	50	288	1.6	16	Chatterjee et al., 2021
γ-ray + EMI + DRS	3,100	73,685	10,850	28,437	398	220	300	380	0.7	–	Malone et al., 2022
γ-ray	1,200	2,685	–	3,935	78	50	15	15	3.3	–	Van Egmond et al., 2018
EMI	1,250	–	–	–	130	195	36	72	5.4	60	Priori et al., 2019
GPR + EMI	714	–	4,463	–	1,035	5	–	–	–	128	Chiarantini et al., 2011
ER	–	–	3,692	–	1,992	5	–	–	–	104	Chiarantini et al., 2011

DRS: diffuse reflectance spectroscopy; γ-ray: gamma-ray spectroscopy; EMI: electromagnetic induction; ER: electrical resistivity; XRF: X-ray fluorescence; GPR: ground-penetrating radar.

Table 11
Summary of quantitative data extracted from the companies' questionnaire replies (n = 24). Data are independent of the PSS technique used. The daily cost of the service includes data analysis and reporting.

Report	Min	Q_1	Median	Q_3	Max
Hectares (ha) per day	4	15	30	100	300
Space (m) between lines	–	13	20	125	250
Cost (€) per hectare (ha)	100	120	142	362	1,300
Cost (€) of the service per day	400	2,575	4,510	7,025	10,070
Cost (€) of renting PSS sensors per day	60	300	300	600	800

(e.g., sensors and materials) in last place. On average, companies attribute 39 % of the total cost to the personnel category, 35 % to the data analysis category, and 11 % to the equipment category (Fig. 12). Fig. 12 illustrates the occurrence of companies voting for each category of cost. First, a consensus was found among the majority of companies assessing the impact of the equipment on the final cost of PSS services, which ranges from 0 to 5 %. Second, 46 % of the companies reported that the cost of data analysis has an impact ranging from 25 to 50 % of the total cost of PSS services. Third, the impact of personnel costs on the final price of PSS services is the most variable, according to the replies of companies, which are homogeneously distributed within the range 5–75 %, with a higher occurrence in the central range.

Around 50 % of companies report that field conditions, rugged morphology, and access difficulties can increase the final cost by 25–50 % (Fig. 13), as these factors affect the number of hectares covered daily. However, it is noteworthy that companies typically notify customers of such cost increases during the quotation phase.

6. Discussion

PA relies on extensive data collection for real-time soil analysis and management. This simple statement is the driving force behind the recent rapid advancement of technology, which enables accurate

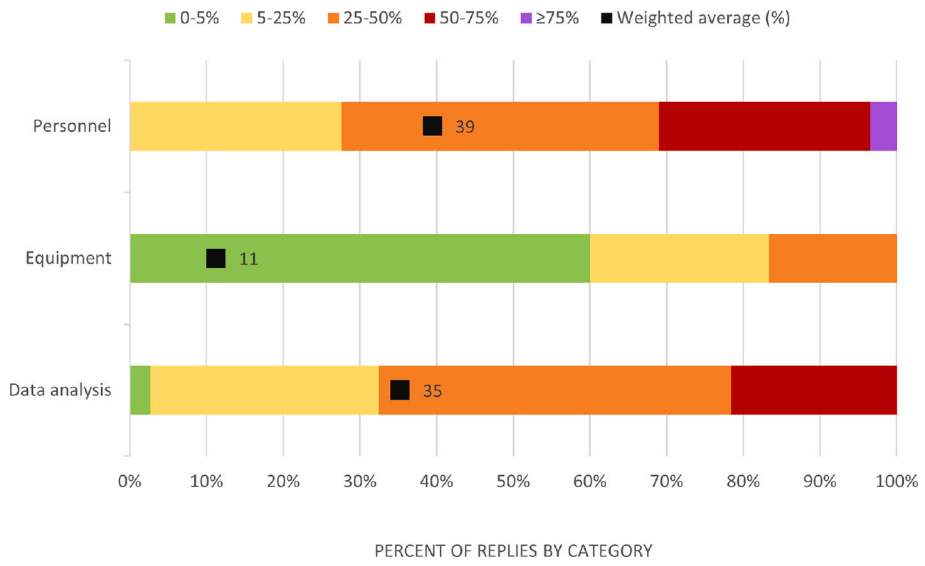

Fig. 12. Assignment of the impact of each single cost category on the final price of a PSS service as provided by companies. Colors represent the impact (i.e., percentage ranges) of each class of cost (i.e., personnel, equipment, and data analysis) on the final cost of the PSS service. The width of each percentage range (colors) within each class of cost bars represents the consensus of companies (i.e., the sum of times that companies assessed specific percentage ranges to each class of cost). For example, in the case of personnel cost, the 28% of companies attributed an impact of personnel cost on the total cost of a PSS service that ranges from 5 to 25% (yellow); the 41% of companies assessed an impact of personnel cost on the total cost of a PSS service that ranges from 25 to 50% (orange); the 28% of companies found consensus in attributing an impact of personnel cost that ranges from 50 to 75% (red) on the total cost of a PSS service; and finally, the 3% of companies declared that the final cost of a PSS services depends up to the 75% on personnel cost (purple). The black squares and the value close to them represent the weighted average of each class of cost, calculated on the basis of the sum of replies by each percentage range, and divided by the total number of replies.

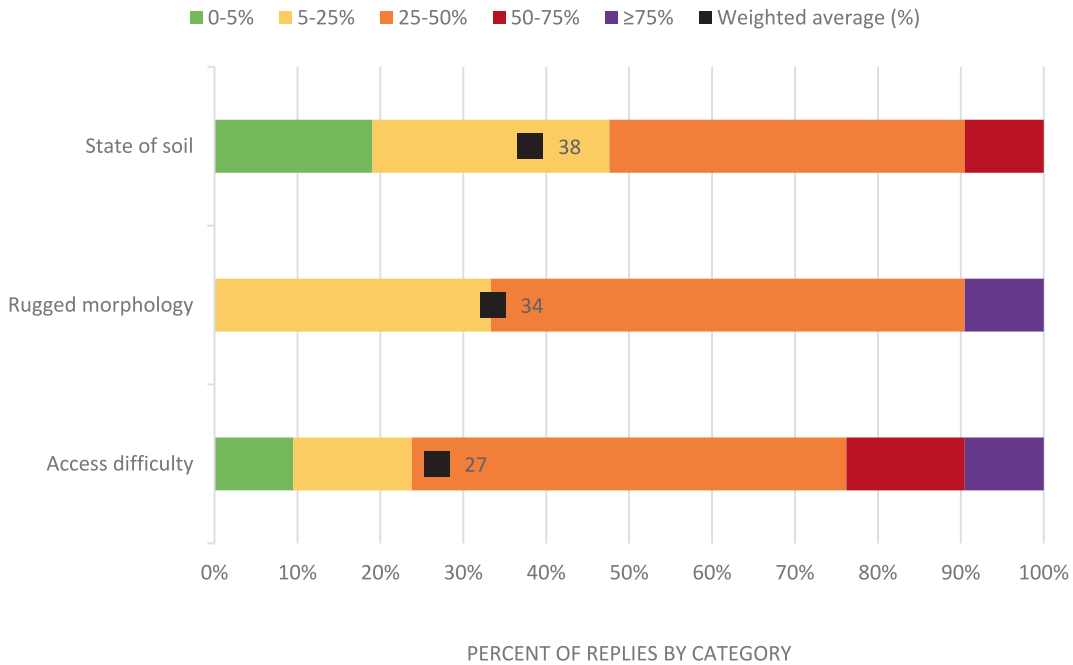

Fig. 13. Assignment of the impact of the different categories of difficulties found during the survey on the final price of a PSS service as reported by companies. Colors represent the weight (i.e., percentage ranges) of each category of impact (i.e., state of soil, rugged morphology, and difficulty of access) on the final cost of the PSS service. The width of each percentage range (colors) within each category of impact bars represents the consensus of companies (i.e., the sum of times that companies assessed specific percentage ranges to each class of cost). For example, in the case of the state of soil, 19% of companies weighted the state of soil's impact on the final cost of PSS services between 0 and 5% (green); 29% of companies weighted the state of soil's impact on the final cost of PSS services between 5 and 25%; 43% of companies weighted the state of soil's impact on the final cost of PSS services between 25 and 50%; and finally, 10% of companies weighted the state of soil's impact on the final cost of PSS services between 50 and 75%. The black squares and the value close to them represent the weighted average of each category of impact, calculated on the basis of the sum of replies by each percentage range, and divided by the total number of replies.

measurements at a reasonable cost. Fundamental research on electromagnetism has brought the possibility of developing portable and affordable electromagnetic sensors that scan signal responses (i.e., PSS proxies), which can be related to physicochemical soil properties and element concentration and, in turn, to soil health and fertility. Establishing relationships between specific properties and the response of

proximal sensors is possible due to calibration and validation analysis. Such relationships can be case-specific, as in the example of spatializing the clay content of agricultural fields using electromagnetic induction, or, instead, less-local calibrations, as it is the implementation of spectral libraries to determine the content of soil samples in SOC and minerals using DRS, for instance. The first case enables farmers to implement smarter crop management, while the second case implies a reduction in time and laboratory materials required for conventional soil analysis (wet chemistry). However, in both cases, the use of PSS proxies implies a significant decrease in the cost associated with enhancing knowledge concerning PA. It is essential to note that PSS does not eliminate the need for soil sampling and analysis but rather significantly reduces the need for multiple soil samples and, subsequently, the cost of laboratory analyses. This led us to the fundamental questions of this systematic review: 1) How much accuracy can we expect from relating PSS proxies to specific soil properties or element concentrations? And 2) how much does it cost to have that information?

6.1. Evaluation of accuracy

6.1.1. Point-based techniques

DRS is the PSS technique that yielded the most accurate average estimations in all the groups of soil properties. The majority of NRMSE records collected in studies using DRS are laboratory measurements; in other words, DRS applications in the field, using handheld portable sensors and spatializations, are underrepresented. However, a significant availability of devices and sensors based on DRS is available for measuring crop health variables, which can be employed for soil monitoring. Our analysis indicates that DRS was able to estimate the most significant number of soil properties compared to the other PSS techniques. The most popular applications of DRS are to determine soil organic matter (or carbon), nutrients, and soil texture. The possibility of creating calibrated models based on SSLs enables the rapid, low-cost, and accurate determination of multiple properties, including acidic-basic properties, soil texture, and nitrogen, using a relatively small number of soil samples (Guerrero et al., 2016; Barbetti et al., 2025). Recent studies have demonstrated the potential of devices like the SoilPRO (Ben-Dor et al., 2017) or NixPro (Cascante et al., 2025) for handheld DRS sensors to collect highly stable measurements of soil surface spectra in the field (see further details in Ben-Dor et al., 2023). Additionally, Castaldi et al. (2025) demonstrated that field spectra can be aligned with spectra in lab-based SSLs, which is a huge advantage for calibration efficiency, despite the influence of soil moisture and surface roughness. Drone-borne multi- and hyperspectral sensors are also popular in soil mapping and soil fertility studies (Crucil et al., 2019). Although DSM with DRS has been tempted by scanning soil cores and profiles, this PSS technique fails to estimate soil properties in the subsoil because the scanning is limited to a few millimeters into the soil surface or the soil sample surface.

After DRS, XRF is the most accurate point-based PSS technique, showing the narrowest standard deviation of NRMSE values. This is presumably due to the sensor calibration performed by the manufacturer. XRF showed the highest average accuracy in estimating properties of the mineralogy and soil texture groups. In a recent and comprehensive review article, Gozukara et al., (2025) also found good accuracy of XRF for sand and clay prediction, although they based their evaluation on R^2 rather than NRMSE. Additionally, XRF demonstrated the highest accuracy in estimating BD, although only one observation was found (Vasques et al., 2020). Most of the collected soil properties estimations are in-field applications with hand-held pXRF sensors, in contrast to DRS. The use of XRF is widespread in determining element concentrations, including nutrients and exchangeable bases, and such properties as cation exchange capacity, acidic-basic properties, nitrogen, and mineralogy. The advantages of the pXRF technique include fast scanning, no sample preparation or destruction required for scanning, no generation of laboratory residues, and a moderate cost of equipment. However, it presents some disadvantages, such as the state of the sample (i.e., moisture, organic matter) causing signal attenuation, dependence of the results on the manufacturer's calibration algorithm, and the low penetration of the X-ray; therefore, as in the DRS, the result of the scanning pertains only to the sample surface (see Ravansari et al., 2020 for further details).

Although most PSS techniques serve multiple purposes, the TDR/FDR technique stands out as the most specific. In fact, all the works considered in this review used TDR and FDR to estimate soil water content. Also, the modeling of TDR/FDR data was limited to linear models. However, this suggests that the TDR and FDR are well-known techniques, with predictions supported by the bibliography, as they require minimal calibration effort. In fact, reflectometry is a technique that accounts for high versatility and applicability in a wide range of environments.

6.1.2. On-the-go techniques

The on-the-go PSS techniques, such as electromagnetic induction and γ-ray spectroscopy, achieved lower accuracy compared to point-based technologies, which is expected due to the type of product generated. Instead, they are highly accurate PSS techniques for producing soil maps, a fact that is highly valuable in PA due to their capacity to define management zones with specific pedological characteristics (Møller et al., 2021) and in water management (Zare et al., 2020). Notably, the application of EMI/ER in crop management is particularly remarkable. Sensors measuring the electrical conductivity of soils and geoelectrical resistivity can be related to derived properties and ecosystem services. An advantage of the EMI sensors is their capacity for 3D mapping. For instance, Zare et al. (2015) successfully estimated soil salinity to a depth of 1 m, whereas Zhao et al. (2019) estimated the clay content up to a depth of 10 m using two EMI sensors.

Γ-ray spectroscopy contributes to PA due to the relationships between radionuclides with water management, soil texture, mineralogy, nutrients, and acidic-basic properties. Similarly, soil carbon has been successfully estimated using γ-ray spectroscopy, yielding highly accurate measurements, despite its apparent independence from radionuclides and organic matter. However, this is possible because of the absorption of organic matter by clay soils. Instead, γ-ray spectroscopy appears to encounter limitations in measurements of the topsoil due to signal attenuation from deeper soil layers. Successful estimations of soil depth and buried cemented layers have been determined with γ-ray sensors. Although γ-ray spectroscopy itself is limited in determining several soil properties, such as soil depth (Koganti et al., 2023), radionuclide concentration is highly correlated with other factors related to weathering, pedogenesis, soil transition, colluvial transport, and alluvial deposition (de Mello et al., 2021).

6.1.3. Imaging techniques (GPR)

Ground Penetrating Radar (GPR) boasts the best resolution among near-surface geophysical technologies. Yet its application in agricultural soils remains confined mainly to identifying soil depth, morphology, horizons, moisture, and underground infrastructure such as drainage or gas pipes (Davis and Annan, 1989; Klotzsche et al., 2018; Koganti et al., 2020; Parry et al., 2014; Pathirana et al., 2023). Although widely used in civil engineering, industrial, and archaeological contexts, the primary reasons for GPR's limited adoption in precision agriculture are its complex data interpretation and the higher cost of surveys compared to EMI and γ-ray methods. Additionally, the GPR's penetration depth can be considerably hampered by the soil's electrical conductivity. The development of customized, drone-mounted GPR systems for topsoil EC or moisture mapping offers a solution, making surveys more affordable and less reliant on GPR specialists (Wu et al., 2019; 2022). However, current regulations significantly constrain these efforts, permitting drone GPR surveys only within 1 m of the terrain. The continued evolution of this technology is contingent on future regulatory changes. Another challenge while working with a GPR is the careful choice of antenna

bandwidths depending on the application needs. There are GPR systems in the market, like stepped frequency continuous wave units (e.g., Koganti et al., 2020), to address this. However, these units are expensive and often can only be afforded by big engineering companies.

6.1.4. Soil spectral libraries (SSLs)

The case of spectral libraries must be considered independently. Since they represent non-local calibrations, the methodology involves distinct steps with specific sources of uncertainty. For example, vis-NIR-SWIR spectra acquired in the field are inherently affected by uncontrolled conditions and, therefore, models trained on SSLs, typically composed of dry, sieved samples analyzed in the lab, often fail when applied directly to field spectra (Castaldi et al., 2025). Other factors that produce uncertainty are the prediction methods. For instance, Zhong et al. (2021) use non-linear convolutional neural networks (i.e., CNNs) for forecasting soil properties with the LUCAS spectral library. Liu et al. (2019) demonstrated that linear models (i.e., PLSR) were unable to predict SOC content in large-scale spectral libraries accurately. However, the GEO-CRADLE spectral library (Tziolas et al., 2019) used local Gaussian regressions (LGR). In fact, investing in the improvement of modeling algorithms allows for better predictions. However, a recent study by Castaldi et al. (2025) has focused on harmonization and spectral pretreatment to align field spectra with lab-based SSLs, a considerable advantage for calibration efficiency. They demonstrated that the conditions in which spectra are collected (i.e., primarily roughness and moisture) have a significant effect on predictions made with SSL, and they propose a routine based on International Soil Standard (ISS) harmonization and the application of External Parameter Orthogonalization (EPO) to mitigate the effects of these disturbing factors. A fact that subsequently improved the prediction of such properties as SOC. Similarly, new efforts found it challenging to estimate soil properties with global SSLs due to the different characteristics of the observations in the SSL and the local data, which cause their conditional and marginal distributions to differ (Viscarra Rossel et al., 2024). Therefore, the authors propose a transfer learning method that uses a small number of SOC values and corresponding spectra collected in local areas to transfer relevant information from large and diverse global SSLs. They found that fewer than 30 local observations produce more accurate and stable estimates of SOC than modelling with only the local data.

Similarly, regional calibration efforts using γ-ray spectra have been employed to predict clay content, utilizing ^{232}Th, in northern Europe (van Egmond et al., 2018) and Mediterranean areas (Coulouma et al., 2016). Similar to vis-NIR SSLs, regional calibrations encounter calibration difficulties related to local characteristics of samples and spatial pedogenetic factors. In γ-ray SSLs, mineralogy, particularly igneous pebbles such as chlorite, is a source of uncertainty (Coulouma et al., 2016).

6.1.5. Combined techniques

The most variable overall accuracy was observed in studies that applied PSS techniques in combination with multi-sensor assets. Additionally, the combination of techniques never showed the highest average accuracy value among all the groups of properties. Presumably, this is due to the additional uncertainty associated with data fusion of PSS proxies. Notwithstanding, specific combinations yielded highly accurate estimations. For example, the combination of TDR with EMI becomes a powerful tool because such an application requires minimum soil sampling, as TDR sensor calibration yields immediate measurements of water content and electrical conductivity. The combination of point-based techniques yields highly accurate estimations of almost the entire spectrum of soil properties considered in this review; however, their estimations are limited to contact with the soil surface. For example, technological advancements introduced portable DRS and XRF sensors in the last few years, enabling operability in the field and facilitating calibration and validation of spectral libraries. Although the almost immediate determination of soil properties in the field (via previous spectral model calibration) is desirable, converting this information into a thematic map of soil properties requires further processing. Our analysis revealed that the most common combination was EMI and γ-ray sensors, primarily focused on determining soil texture, soil depth, identifying cemented layers, hydrological behavior of fields, salinity, nutrients, exchangeable bases, and clay content and mineralogy. The combination of DRS and TDR sensors yielded highly accurate estimations of hydrological properties; however, they are point-based. On the other hand, DRS spectra and modeling can be successfully applied to accurately obtain soil property information and provide sufficient input for DSM, as demonstrated by Zhang et al. (2020), as well as indicated by our analysis, which identified the combination of DRS and EMI to be a good strategy to estimate soil texture.

The integration of point-based and on-the-go PSS techniques offers a powerful strategy to improve soil property estimation and DSM, balancing the high accuracy of discrete measurements from sensors such as TDR, portable DRS, and XRF with the continuous spatial coverage provided by on-the-go instruments like EMI, γ-ray, and multi-sensor arrays (Wangeci et al., 2024; Loria et al., 2024; Schmidinger et al., 2024; Grunwald et al., 2024). While data fusion can introduce additional uncertainty, specific combinations, such as TDR with EMI or DRS with EMI, enable rapid, field-based estimation of water content, electrical conductivity, soil texture, clay mineralogy, and salinity with minimal soil sampling (Musa et al., 2024; Zhang et al., 2024). Local calibration approaches provide high-precision, site-specific predictions that account for micro-scale heterogeneity, whereas global calibration models leverage multi-region datasets for broader applicability but may introduce additional uncertainty due to soil-type and environmental variability (Hutengs et al., 2024; Batjes et al., 2024; Filippi et al., 2024). Advances in machine learning, including transfer learning and ensemble modeling, allow integration of local and global calibration schemes, improving predictive accuracy and facilitating the creation of high-resolution, spatially explicit soil property maps that support precision agriculture, carbon accounting, and ecosystem management (Grunwald et al., 2024; Rosso et al., 2025).

6.2. Factors influencing the outcomes of proximal soil sensing

The accuracy with which a specific soil property is estimated using any PSS technique not only depends on the sensor but rather is the result of a step-by-step process that combines the selection of sampling locations, soil sampling and fieldwork, accuracy of wet chemistry analyses, and calibration and validation of statistical models. Any step is subject to inherent sources of error that influence the overall accuracy of the process.

It is essential to emphasize that the general predictive ability of mobile sensors is dependent on soil spatial variability, as well as the concentrations and ranges of soil properties (Knadel et al., 2015). The employed models have a substantial impact on the estimations, as demonstrated by our analysis. In modeling studies using DRS, specific data preprocessing steps, such as calculating spectral derivatives (Hong et al., 2019), spectral scatter correction, and continuum removal preprocessing, enhance the predictions of soil properties, particularly SOC (Carnieletto et al., 2018). From our analysis, it can be inferred that overall, there is no clear differentiation between estimations of soil properties obtained using non-linear modeling and DRS compared to those obtained with linear models. However, the differentiation is evident when examining the individual properties. Properties that are difficult to estimate, such as bulk density and acidic-basic properties, seem to respond better to non-linear modeling compared to properties that have known spectral signatures, which achieve better estimations with linear modeling. In general, LM outperformed NLM, but a strong effect on the accuracy of including covariates was identified in the group of NLM records.

In DSM studies that employ several on-the-go PSS techniques, such as

EMI and γ-ray, comparisons have been conducted between linear, non-linear, and hybrid modeling (i.e., linear or non-linear regressions to analyze trends and then kriging the residuals). Results showed that the accuracy of estimations varied, of course, depending on the modeling technique applied, the number of covariates used, and the number of samples used for calibration (Arshad et al., 2021). What is noteworthy is that the effect of these factors on the accuracy of the estimations appears to be case-specific; in other words, accuracy varied strongly depending on the property being estimated and the local characteristics of the field, a key difference from predicting properties using SSLs. For instance, studies have been conducted to predict soil properties in fields using models calibrated in adjacent fields, with negative results (Triantifilis et al., 2024). Besides, several studies have noted that a minimum of 30 soil samples is required to obtain acceptable prediction models (Koganti et al., 2023). We found that the accuracy of soil property estimation using NLMs generally improves with an increase in the number of samples and with the moderate addition of covariates. In contrast, the addition of covariates appears to have a noisy effect on the estimation of soil properties using LMs.

In the PA context, the accuracy of soil property spatializations using PSS can be influenced by management practices and the time of year when surveys are conducted (i.e., the soil's condition), as demonstrated by Pedrera-Parrilla et al. (2016). It is expected that more accurate results will be achieved at the soil surface due to the uniform environment in the plow layer (Zhang et al., 2020). Additionally, various sensors have different limitations in different environments, and thus, PSS largely relies on site-specific calibrations after pre-processing or applying correction algorithms to the collected data.

6.3. Cost of proximal soil sensing from different perspectives

6.3.1. Research perspective

The literature review on cost highlights several efforts to analyze the cost structure of PSS applications. Chatterjee et al. (2021) examined various cost components, including hardware or rental expenses, data preprocessing and analysis, and modeling and mapping. Additionally, authors focused on combining proximal sensors with morphometric and remote sensing covariates, resulting in maps of land management zones with reasonable accuracy while maintaining moderate survey costs. For a complete and rapid digital soil mapping of 80 ha, the reported cost is 1,250 € (15.50 €/ha). This amount, excluding traditional soil analysis costs, is divided as follows: rental cost (450 €), preprocessing cost (530 €), and modeling cost (270 €), with a total working time of 16 h. Malone et al. (2022) reported the total cost per hectare of ~ 400 € for a rapid and granular farm landscape characterization with a sample density of 0.7/ha. This detection includes on-the-go proximal soil surveys, soil core sampling and scanning, soil analysis (190 € per sample), and subsequent data analysis and modeling to create 3D-like digital soil attribute maps. These two authors agree on the significant advantage of using proximal sensors compared to traditional soil surveys, estimating a gain of ~ 80 %. The technical report by van Egmond et al. (2018) describes an advantageous process that utilizes moving gamma radiation to determine the texture of topsoil. The effectiveness of this method is due to utilizing existing libraries rather than collecting and analyzing new samples. This approach may reduce the cost per hectare by a factor of between 3 and 10. Priori et al. (2019) observed, through a market survey, that the total costs of high-detail soil surveys using PSS are primarily dependent on the size of the investigation area. For instance, using a case study of 195 ha with an EMI sensor, the authors reported a cost of approximately 130 €/ha, with a sampling density of 5.4 samples per hectare. Although the work of Chiarantini and Diafas (2011) is no longer aligned with current market trends, it remains a milestone in estimating the cost-effectiveness of digital soil mapping.

For point-based measurements, Li et al. (2022) proposed an equation that calculates the cost-effectiveness of spectroscopy, based on the number of samples; the data acquisition capacity and the laboratory capacity to prepare samples for analysis or spectroscopy, the accuracy of measurements based on the mean squared error (MSE), and compares the whole process to the cost of the dry combustion method, considering several spectroradiometers. The authors analytically demonstrated that spectroscopy is a reliable alternative, reducing costs by more than 60 % compared to conventional laboratory methods. Similarly, England and Viscarra Rossel et al. (2018) reported a unit cost of 5 € for vis-NIR analysis of dried ground samples and 9 € for mid-IR analysis of dried, finely ground samples.

However, a common trait across these studies is the implementation of high spatial and temporal resolution soil assessments. While scientifically valuable, such approaches result in costs that are too high from the standpoint of most small-scale farmers and agricultural companies.

6.3.2. Company perspective

Accurate information on the costs of PA services is scarce in the literature, making it challenging to draw reasonable comparisons. However, we found that the average cost per hectare surveyed is around 375 €, with a minimum of 100 € when using motorized platforms, according to private companies. The price per hectare can be even lower if flying platforms such as UAVs are used. This aligns with current market trends and the literature referenced earlier. Unfortunately, estimating the costs of soil surveys remains uncertain and variable, depending on the survey's aim, the number of data collected, the specifics of fieldwork, and difficulties. However, we identified two main factors that allow PSS surveys to be comparable: the scale of the study and sampling density.

Costs can be divided into three broad classes: 1) Fieldwork, including the acquisition with proximal sensors, soil sampling, rental costs and possibly the depreciation cost share of the instruments; 2) preparation and preprocessing including the selection of survey sites, the processing and treatment of the data collected in the field, and the costs of laboratory analysis; 3) the modeling and reporting including the production of outputs through modeling with model validation, calibration, and map generation.

Companies declare that the final price includes equipment, personnel, and data analysis costs, but excludes costs derived from vehicles, such as tractors, fuel, and driver expenses. That fact could increase the final price by up to 30 %. Costs can vary significantly due to difficulties that may arise during surveys, primarily concerning accessibility, the state of growth and crop cycle, the state of the soil due to harsh meteorological conditions, and rugged morphology, which often imply an extra charge in the final price. However, such modifications to the final cost were previously communicated by companies. The cost of mapping services is also affected by geographic areas. For example, the time of year when the survey is conducted is significant for how much can be mapped in a single field day, given the hours of daylight available in high-latitude countries. In fact, the daily surveyed area conducted during the summer can double the daily surveyed area if conducted during the winter season. In Denmark, some companies have declared a 10 % price increase due to difficulties accessing the fields. Still, in other Scandinavian countries with mountains, the increase is much higher. Other companies declare that they do not charge extra for accessibility difficulties, but such replies were associated with companies that primarily used flying platforms for surveying in more temperate regions. Personnel and data analysis costs are often more significant than equipment costs because they are typically adequately covered during the useful life of the instruments.

Based on the replies to the questionnaires, we deduced that the reporting of results is rarely linked to accuracy or uncertainty values, probably because performing such an analysis requires a larger number of soil samples. This fact would have a direct impact on the final price of the service. Data policy is a sensitive matter among companies. For example, some companies have open data policies, providing customers with full access to raw data, whereas others are closed about the data, interpretations, and algorithms employed. This fact seems to create disagreement among companies. Finally, companies regret that the

majority of farmers lack interest in mapping services, a fact that impacts the sector's business efficiency.

6.3.3. Client perspective

A detailed economic evaluation approach was developed to probe and assess the willingness-to-pay (WTP) of potential users of digital soil maps, as part of the European DIGISOIL project (Diafas et al., 2013). WTP can be defined as the maximum amount someone is willing to pay for a product or service (Diafas et al., 2013). According to the results of Chiarantini and Diafas (2011) WTP depends on the resolution and stated accuracy of digital soil maps for key soil properties. For example, the average end user would be WTP 263 € per hectare for a low-accuracy measurement of carbon content. However, the same users would be WTP 789 € per hectare (three times the previous cost) for a highly accurate measurement. Instead, the low demand by farmers for soil mapping services may stem from harmful practices and the provision of poor-quality products, sometimes in exchange for an excessive amount of money. Word of mouth can negatively influence farmers' perception of digital soil mapping products.

6.4. Future perspectives and challenges

Future developments in PSS and DSM will depend on extending the applicability of sensing technologies across a broader spectrum of soil types, climatic regions, and management systems. This requires extensive, harmonized calibration datasets and coordinated validation frameworks to avoid inappropriate use and growing user skepticism (Najdenko et al., 2024; Batjes et al., 2024; Hengl et al., 2025). Some soil properties, such as bulk density and soil compaction, remain difficult to predict reliably, despite decades of work with passive γ-ray detection (van Egmond et al., 2024; Carrera et al., 2024). Emerging active γ-ray systems offer a promising alternative but face regulatory hurdles and a need for extensive cross-regional calibration (van Egmond et al., 2024). In parallel, new sensor families ranging from portable LIBS (laser induced breakdown spectroscopy), microwave, and spectrofluorometric devices to magnetic susceptibility meters and cosmic-ray neutron probes are rapidly maturing and will likely enter routine monitoring pipelines once robust comparative benchmarks are established (Wigneron et al., 2017; Wangeci et al., 2024; Loria et al., 2024; Gianessi et al., 2024; Zhang et al., 2024). These advances coincide with the rise of integrated multi-sensor platforms and low-cost wireless networks, which may finally enable reliable, real-time transmission of high-resolution soil data from mobile platforms, something currently feasible only for stationary systems (Musa et al., 2024; Tu et al., 2022; Schmidinger et al., 2024). Emerging sensor models are expected to expand the PSS toolbox beyond established electromagnetic techniques, with adoption driven by comparative benchmarks, cross-site calibration robustness, and regulatory acceptance rather than by technological novelty alone.

The fusion of PSS and remote sensing is expected to become a cornerstone of future soil monitoring and measurement, reporting, and verification (MRV) systems for soil carbon and other ecosystem services. Recent satellite missions (e.g., Sentinel-2, PRISMA, EnMAP, SAR constellations) have demonstrated strong potential for large-scale spatialization of soil properties and land-management characterization (Zhou et al., 2025; Filippi et al., 2024). Yet, remote sensing alone still produces sub-optimal predictions; the most promising advances emerge when proximal, UAV-borne, tractor-mounted, or robotic sensors are integrated with multispectral, hyperspectral, and radar observations (Schmidinger et al., 2024). Multi-tier verification frameworks, such as those described for carbon MRV by Batjes et al. (2024) and operationalized in MARVIC and MRV4SOC, illustrate how modular data fusion can enhance both accuracy and transparency. Examples from archaeology and geoheritage, such as mapping extinct Nile branches using radar imagery calibrated with GPR and electromagnetic tomography (EMT) surveys, highlight the broader cross-disciplinary utility of such combined approaches (Ghoneim et al., 2024). Future soil monitoring frameworks are expected to increasingly rely on hierarchical fusion of PSS, UAV, and satellite data, leveraging the complementary strengths of local accuracy and large-scale spatial coverage.

Rapid progress in artificial intelligence (AI) will further shape the next generation of soil sensing applications. Machine learning, deep neural networks, and transfer-learning architectures are increasingly effective at modelling nonlinear relationships between heterogeneous sensor signals and soil properties, improving both prediction accuracy and uncertainty quantification (Hutengs et al., 2024; Grunwald et al., 2024). These methods also enable more adaptive, real-time DSM workflows compatible with autonomous systems, including UAVs, ground robots, and smart tractors (Rosso et al., 2025). To ensure adoption, however, the field must address interoperability, user-centric tool design, and integration of PSS data into decision-support systems. Modular decision-tree frameworks (van Egmond et al., 2024) exemplify how complex methodological choices can be translated into intuitive guidance for practitioners. Ultimately, the future of PSS will depend on bridging technological innovation with regulatory clarity, transparent MRV requirements, and user-friendly tools that translate sensing outputs into operational decisions for precision agriculture, carbon accounting, and environmental monitoring. Henceforth, the long-term impact of PSS innovations will depend on their alignment with MRV requirements, regulatory frameworks such as the new Soil Monitoring Law in the European Union (Directive (EU) 2025/2360, 2025), and standardized reporting protocols that ensure traceability, comparability, and user trust.

7. Concluding remarks

Since one of the future PA needs relies on the use of in situ and on-the-go sensors without sample preparation, this review guides the selection among the wide range of possible sensor combinations, remote and terrain data for the accurate estimation of soil properties, and precision soil mapping. The broad overview of this work has identified critical aspects influencing the accuracy involved in PSS surveys. We identified that point-based measurements are more accurate with respect to on-the-go techniques. However, the choice of technique to use depends primarily on the purpose of the survey. Notably, our analysis determined the best combination of factors yielding more accurate estimations for each soil property and under which conditions. Additionally, we argue why some highly accurate techniques can give imprecise outcomes depending on the situation. In fact, it is essential to keep in mind that proximal sensor data measures bulk properties of soils rather than individual properties (Kerry and Escolà, 2021). Therefore, outcomes require expert interpretation.

Questionnaires highlighted the extent of uptake of some technologies among precision agriculture-focused companies, such as electromagnetic induction, when providing mapping services. Some companies are technologically well-equipped with new-generation sensor types, e.g., Cosmic Ray Neutron Sensor (CRNS) for detecting soil moisture. EMI is the most popular PSS technique in the industry. Despite the accuracy of point-based soil spectroscopy (i.e., DRS) and x-ray fluorescence (XRF), there are still few companies investing in such technologies. Similarly, investments of companies in γ-ray technology were not frequent despite the accuracy of soil mapping products. Instead, many companies relied on DRS-based on-the-go sensors supplied by Veris Technologies for determining soil and crop properties.

Regarding cost, we identified that it varies strongly. Based on the replies to our questionnaire, the price of a surveyed hectare is between 120 and 362 €, whereas the customers' willingness to pay for having precision information of their fields rounds, on average, 789 €/ha, based on the literature. The factors that affect variation in the cost of PSS services are the platform employed for sensing (i.e., the number of hectares covered per day), the required personnel, the number of samples collected for validation, and factors related to accessibility, such as the state of the terrain and morphology, or the distance to the area of

interest.

Our study reveals that the efficiency of soil mapping services has significantly improved over the past decade, primarily due to the adoption of open-source software, including GIS tools for modeling, artificial intelligence, and advancements in sensors and data acquisition techniques. These developments have significantly reduced the time required for data processing, which is directly related to the growth trends in PA.

Looking ahead, several challenges and opportunities emerge from this work. This systematic review provided a structured and transparent synthesis of the available evidence, capturing the diversity of sensor types, measurement conditions, and outcomes reported across studies. By not requiring the strict data availability criteria needed for quantitative aggregation, it includes a broader spectrum of literature that other types of review approaches, such as the *meta*-analysis (Page et al., 2021), thereby offering a very comprehensive overview of the current landscape. Future research could build on this foundation through a dedicated *meta*-analysis to quantitatively integrate performance metrics and explore the sources of variability across studies. Moreover, it will be important to extend the same level of assessment applied here (of particular relevance to the ProbeField Project) to sensor technologies not covered in the present review, and to update and expand the economic analysis for both established and emerging techniques. It could be supported by newly available literature or further questionnaire data, and would also help strengthen the evidence base, guide future technological development, and adoption in precision soil sensing.

CRediT authorship contribution statement

Carlos Lozano-Fondón: Writing – review & editing, Writing – original draft, Methodology, Investigation, Formal analysis, Data curation, Conceptualization. **Romina Lorenzetti:** Writing – review & editing, Writing – original draft, Methodology, Investigation, Funding acquisition, Formal analysis, Data curation, Conceptualization. **Roberto Barbetti:** Writing – review & editing, Writing – original draft, Methodology, Investigation, Formal analysis, Data curation, Conceptualization. **Konrad Metzger:** Writing – review & editing, Writing – original draft, Methodology, Investigation, Formal analysis, Data curation, Conceptualization. **Gabriele Buttafuoco:** Writing – review & editing, Writing – original draft, Methodology, Investigation, Formal analysis, Data curation, Conceptualization. **Melis Özge Pinar:** Writing – review & editing, Writing – original draft, Methodology, Investigation, Formal analysis, Data curation, Conceptualization. **Sevinç Madenoğlu:** Writing – review & editing, Writing – original draft, Methodology, Investigation, Formal analysis, Data curation, Conceptualization. **Taru Sandén:** Writing – review & editing, Writing – original draft, Methodology, Investigation, Formal analysis, Data curation, Conceptualization. **Asa Gholizadeh:** Writing – review & editing, Writing – original draft, Methodology, Investigation, Formal analysis, Data curation, Conceptualization. **Bo Stenberg:** Writing – review & editing, Writing – original draft, Methodology, Investigation, Formal analysis, Data curation, Conceptualization. **Maria Fantappiè:** Writing – review & editing, Writing – original draft, Methodology, Investigation, Formal analysis, Data curation, Conceptualization. **Fenny van Egmond:** Investigation. **Frank Liebisch:** Writing – review & editing, Writing – original draft, Methodology, Investigation, Formal analysis, Data curation, Conceptualization. **Rafael López Núñez:** Writing – review & editing, Writing – original draft, Methodology, Investigation, Formal analysis, Data curation, Conceptualization. **Maria Knadel:** Writing – review & editing, Writing – original draft, Methodology, Investigation, Formal analysis, Data curation, Conceptualization. **Triven Koganti:** Writing – review & editing, Writing – original draft, Methodology, Investigation, Formal analysis, Data curation, Conceptualization.

Declaration of competing interest

The authors declare that they have no known competing financial interests or personal relationships that could have appeared to influence the work reported in this paper.

Acknowledgements

This work has been carried out with funding from the European Union's Horizon 2020 Research and Innovation Program under Grant Agreement N° 862695, and from the Tillämpninggsklivet Precisionsodling RUN 2021-00020 Region Västra Götaland.

The authors would like to express their special thanks to all the PSS companies that collaborated by answering to the questionnaire and sharing their experience with this study (in alphabetical order: AGRICOLUS, AgroDato, Agronica IBF, AgroScan 4.0, ARVAtec, Ekoton, Finapp, GPS Agro, Geoprospectors, LandScan, Medusa, METOS TR, NIRAS, Opticultures, Raimond, SARICON, Soil Masters, SOING, and Veris Technologies) and, of course, to those who preferred remaining anonymous. The authors also thank all their colleagues in the ProbeField Project and the EJPSOIL program in general for their contribution to this study. Finally, the authors thank the reviewers of this paper for providing constructive comments, which have contributed to the improvement of the published version.

Appendix A. Supplementary material

Supplementary data to this article can be found online at https://doi.org/10.1016/j.compag.2025.111378.

Data availability

We have shared the used dataset, adding the link of repository in the manuscript (https://doi.org/10.5281/zenodo.17121809).

References

Aarif, K.O., Mohammed, A., Afroj, H., Yousuf, 2025. Smart sensor technologies shaping the future of precision agriculture: recent advances and future outlooks. J. Sens. 2460098. https://doi.org/10.1155/js/2460098.

Abdu, H., Robinson, D.A., Jones, S.B., 2007. Comparing bulk soil electrical conductivity determination using the DUALEM-1S and EM38-DD electromagnetic induction instruments. Soil Sci. Soc. Am. J. 71 (1), 189–196.

Adamchuk V., Biswas A., Huang H.H., Holland J., Taylor James., Stenberg B., Wetterlind J., Singh K., Minasny B., Fidelis C., Yinil D., Sanderson T., Snoeck D., Field D., 2021. Soil Sensing. 10.1007/978-3-030-78431-7_4.

Adamchuk, Viacheslav, Ji, Wenjun, Viscarra Rossel, Raphael, Gebbers, Robin, Tremblay, Nicolas, Shannon, D.K., Clay, David, Kitchen, N.R., 2018. Proximal Soil and Plant Sensing. 10.2134/precisionagbasics.2016.0093.

Adamchuk, V.I., Christenson, P.T., 2005. In: Stafford, J. (Ed.), An integrated system for mapping soil physical properties on-the-go: the mechanical sensing component. The 5th European Conference on Precision Agriculture proceedings. Wageningen Academic Publishers, Wageningen. The Netherlands, pp. 449–456. https://doi.org/10.3920/9789086865499_056.

Antonangelo, J., Zhang, H., 2024. Assessment of portable X-ray fluorescence (pXRF) for plant-available nutrient prediction in biochar-amended soils. Sci. Rep. 14, 20377. https://doi.org/10.1038/s41598-024-71381-8.

Arshad, R.N., Abdul-Malek, Z., Roobab, U., Munir, M.A., Naderipour, A., Qureshi, M.I., Aadil, R.M., 2021. Pulsed electric field: a potential alternative towards a sustainable food processing. Trends Food Sci. Technol. 111, 43–54.

Barbetti, R., Palazzi, F., Chiarabaglio, P.M., Fondon, C.L., Rizza, D., Rocci, A., Grignani, C., Zavattaro, L., Moretti, B., Fantappiè, M., Monaco, S., 2025. Can Soil Organic Carbon in Long-Term Experiments Be Detected Using Vis-NIR Spectroscopy? IEEE Trans. AgriFood Electr. 3, 43–48. https://doi.org/10.1109/TAFE.2024.3449215.

Barra, I., Haefele, S.M., Sakrabani, R., Kebede, F., 2021. Soil spectroscopy with the use of chemometrics, machine learning and pre-processing techniques in soil diagnosis: recent advances – a review. TrAC Trends Anal. Chem. 135 (2021), 116166. https://doi.org/10.1016/j.trac.2020.116166.

Batjes, N.H., Ceschia, E., Heuvelink, G.B.M., Demenois, J., le Maire, G., Cardinael, R., Arias-Navarro, C., van Egmond, F., 2024. Towards a modular, multi-ecosystem monitoring, reporting and Verification (MRV) framework for soil organic carbon stock change assessment. Carbon Manage. 15 (1). https://doi.org/10.1080/17583004.2024.2410812.

Beckhoff, B., Kanngießer, B., Langhoff, N., Wedell, R., & Wolff, H. (Eds.)., 2007. Handbook of practical X-ray fluorescence analysis. Springer Science & Business Media.

Bellon-Maurel, V., McBratney, A., 2011. Near-infrared (NIR) and mid-infrared (MIR) spectroscopic techniques for assessing the amount of carbon stock in soils - critical review and research perspectives. Soil Biol. Biochem. 43 (2011), 1398–1410.

Ben-Dor, E., Granot, A., Notesco, G., 2017. A simple apparatus to measure soil spectral information in the field under stable conditions. Geoderma 306, 73–80. https://doi.org/10.1016/j.geoderma.2017.06.025.

Ben, D.E., Granot, A., Wallach, R., Francos, N., Pearlstein, H.D., Efrati, B., Borůvka, L., Gholizadeh, A., Schmid, T., 2023. Exploitation of the SoilPRO® (SP) apparatus to measure soil surface reflectance in the field: five case studies. Geoderma 438, 116636. https://doi.org/10.1016/j.geoderma.2023.116636.

Bradford, J.H., 2007. Frequency-dependent attenuation analysis of ground-penetrating radar data. Geophysics 72, J7–J16.

Brodsky, L., Vašát, R., Klement, A., Zádorová, T., Jaksik, O., 2013. Uncertainty propagation in VIS-NIR reflectance spectroscopy soil organic carbon mapping. Geoderma 199, 54–63. https://doi.org/10.1016/j.geoderma.2012.11.006.

Brown, D., Shepherd, K., Walsh, M., Mays, M., Reinsch, T., 2006. Global soil characterization with VIS-NIR diffuse reflectance spectroscopy. Geoderma 132, 273–290. https://doi.org/10.1016/j.geoderma.2005.04.025.

Ben-Dor E., Ong C., Lau I.C., 2015. Reflectance measurements of soils in the laboratory: Standards and protocols, Geoderma, Volumes 245–246,2015, Pages 112-124, ISSN 0016-7061, Doi: 10.1016/j.geoderma.2015.01.002.

Carnieletto D.A., Diniz Dalmolin R.S., ten Caten A., Grunwald S., 2018. A systematic study on the application of scatter-corrective and spectral-derivative preprocessing for multivariate prediction of soil organic carbon by Vis-NIR spectra. Geoderma 314, pages 262-274. DOI: 10.1016/j.geoderma.2017.11.006.

Carrera, A., Peruzzo, L., Longo, M., Cassiani, G., Morari, F., 2024. Uncovering soil compaction: performance of electrical and electromagnetic geophysical methods. Soil 10, 843–857. https://doi.org/10.5194/soil-10-843-2024.

Cascante, M.D., Wu, P.-H., Asio, V.B., Yanai, J., Hseu, Z.-Y., 2025. Low-cost proximal sensors for assessing organic carbon and potentially toxic metals in highly weathered soils: a systematic review. Soil Secur. 21, 100208. https://doi.org/10.1016/j.soisec.2025.100208.

Cassidy N.J., 2009a. Electrical and magnetic properties of rocks. soils and fluids. In: Jol. H.M. (Ed.). Ground Penetrating Radar: Theory and Applications. Elsevier Science. Amsterdam. pp. 41-67.

Castaldi, F., Stenberg, B., Liebisch, F., Metzger, K., Ben-Dor, E., Knadel, M., Koganti, T., Wetterlind, J., Barbetti, R., Debaene, G., Klumpp, K., Lippl, M., Lorenzetti, R., Lozano Fondon, C., Sanden, T., Schaumberger, A., Stajnko, D., 2025. Estimating soil organic carbon using field VNIR-SWIR spectroscopy and existing soil spectral libraries: Mitigating heterogeneity, roughness and moisture effects. Smart Agric. Technol. 12, 101353. https://doi.org/10.1016/j.atech.2025.101353.

Chang, R., Fu, B., Liu, G., Liu, S., 2011. Soil carbon sequestration potential for “grain for green” project in Loess Plateau, China. Environ. Manage. 48, 1158–1172. https://doi.org/10.1007/s00267-011-9682-8.

Chatterjee S. Hartemink A.E., Triantafilis J., Desai A. R., Soldat D., Zhu L., Townsend P. A., Zhang J., Huang J., 2021. Characterization of field-scale soil variation using a stepwise multi-sensor fusion approach and a cost-benefit analysis. CATENA. Volume 201.2021. 105190. ISSN 0341 8162. Doi: 10.1016/j.catena.2021.105190.

Chiarantini, L., Diafas, I., 2011. Evaluation with respect to the cost effectiveness. Report N° FP7-DIGISOIL-D4.3; 21 pages.

Clairotte, M., Grinand, G., Kouakoua, E., Thébault, A., Saby, N.P., Bernoux, M., Barthès, B.G., 2016. National calibration of soil organic carbon concentration using diffuse infrared reflectance spectroscopy. Geoderma 276 (2016), 41–52.

Conyers, L.B., 2004. Ground penetrating radar for archaeology. J. Field Archaeol. 31, 105–107. https://doi.org/10.2307/40024722.

Cook, S.E., Corner, R.J., Groves, P.R., Grealish, G.J., 1996. Use of airborne gamma radiometric data for soil mapping. Aust. J. Soil Res. 34 (1), 183–194.

Comas, X., Terry, N., Slater, L., Warren, M., Kolka, R., Kristiyono, A., Sudiana, N., Nurjaman, D., Darusman, T., 2015. Imaging tropical peatlands in Indonesia using ground-penetrating radar (GPR) and electrical resistivity imaging (ERI): implications for carbon stock estimates and peat soil characterization. Biogeosciences 12, 2995–3007.

Corwin, D.L., Lesch, S.M., 2003. Application of soil electrical conductivity to precision agriculture: theory. principles. and guidelines. Agron. J. 95, 455–471.

Coulouma, G., Caner, L., Loonstra, E.H., Lagacherie, P., 2016. Analysing the proximal gamma radiometry in contrasting Mediterranean landscapes: towards a regional prediction of clay content. Geoderma 266, 127–135. https://doi.org/10.1016/j.geoderma.2015.12.006.

Crucil, G., Castaldi, F., Aldana-Jagüe, E., van Wesemael, B., Macdonald, A., Van Oost, K., 2019. Assessing the performance of UAS-compatible multispectral and hyperspectral sensors for soil organic carbon prediction. Sustainability 11 (7), 1889. https://doi.org/10.3390/su11071889.

Dalton, F.N., Herkelrath, W.N., Rawlins, D.S., Rhoades, J.D., 1984. Time-domain reflectometry: simultaneous measurement of soil water content and electrical conductivity with a single probe. Science 224 (4652), 989–990.

Davis, J.L., Annan, A.P., 1989. Ground-penetrating radar for high-resolution mapping of soil and rock stratigraphy 1. Geophys. Prospect. 37 (5), 531–551.

Davis J.L., Chudobiak W.J., 1975. In situ meter for measuring relative permittivity of soils. Doi: 10.4095/104349.

de Mello, D.C., Demattê, J.A.M., de Oliveira, M.F.A., Poppiel, R.R., Quiñonez, N.E., Safanelli, J.L., de Souza, B.A., di Loreto di Raimo, L.A., Rizzo, R., Bispo Resende, M. E., Gonçalves Reynaud Schaefer, C.E., 2021. Applied gamma-ray spectrometry for evaluating tropical soil processes and attributes. Geoderma 381, 114736. https://doi.org/10.1016/j.geoderma.2020.114736.

Directive (EU) 2025/2360 of the European Parliament and of the Council of 12 November 2025 on soil monitoring and resilience (Soil Monitoring Law). Official Journal of the European Union, L 336, 1–xx. https://eur-lex.europa.eu/eli/dir/2025/2360/oj.

Diafas, I., Panagos, P., Montanarella, L., 2013. Willingness to Pay for Soil Information Derived by Digital Maps: A Choice Experiment Approach. Vadose Zone Journal 12, 1–8. https://doi.org/10.2136/vzj2012.0198.

Dirksen, C., Dasberg, S., 1993. Improved calibration of time domain reflectometry soil water content measurements. Soil Sci. Soc. Am. J. 57 (3), 660–667. https://doi.org/10.2136/sssaj1993.03615995005700030005x.

Dobson, M., Ulaby, F., Hallikainen, M., El-rayes, M., 1985. Microwave dielectric behavior of wet soil-Part II: Dielectric mixing models. IEEE Trans. Geosci. Remote Sens. GE-23(1), 35–46. https://doi.org/10.1109/TGRS.1985.289498.

Duda B.M., Weindorf D.C., Chakraborty S., Li B., Man T., Paulette L., Deb S., 2017. Soil characterization across catenas via advanced proximal sensors, Geoderma, Volume 298, , Pages 78-91, ISSN 0016-7061, Doi: 10.1016/j.geoderma.2017.03.017.

England, J.R., Viscarra Rossel, R.A., 2018. Proximal sensing for soil carbon accounting. Soil 4, 101–122. https://www.soil-journal.net/4/101/2018. https://doi.org/10.5194/soil-4-101-2018.

Everett M.E., 2013a. Electromagnetic induction. Near-surface applied geophysics. Cambridge University Press. New York. pp. 200-238.

Everett M.E., 2013b. Ground-penetrating radar. Near-surface applied geophysics. Cambridge University Press. New York. pp. 239-277.

de Faria, A.J.G., Silva, S.H.G., Andrade, R., Mancini, M., Melo, L.C.A., otros, 2022. Prediction of soil organic matter content by combining data from Nix pro™ color sensor and portable X-ray fluorescence spectrometry in tropical soils. Geoderma Reg. 28, e00461. https://doi.org/10.1016/j.geodrs.2021.e00461.

Fedeli, R., Di Lella, L.A., Loppi, S., 2024. Suitability of XRF for routine analysis of multi-elemental composition: a multi-standard verification. Methods and Protocols 7 (4), 53. https://doi.org/10.3390/mps7040053.

Ferré, P.A., Topp, G.C., 2000. Time-domain reflectometry techniques for soil water content and electrical conductivity measurements. Sensors Update 7 (1), 277–300. https://doi.org/10.1002/1616-8984(200001)7:1<277::AID-SEUP277>3.0.CO;2-M.

Filippi, P., Whelan, B.M., Bishop, T.F., 2024. Proximal and remote sensing–what makes the best farm digital soil maps? Soil Res. 62 (2).

Fulajtar, E., Mabit, Lionel & Renschler, Chris, Lee Zhi Yi, Amelia. (2017). Use of 137Cs for soil erosion assessment.

Gebbers, R., Adamchuk, V.I., 2010. Precision agriculture and food security. Science 327 (5967), 828–831. https://doi.org/10.1126/science.1183899.

Ghoneim, E., Ralph, T.J., Onstine, S., El-Behaedi, R., El-Qady, G., Fahil, A.S., Fathy, M.S., 2024. The Egyptian pyramid chain was built along the now abandoned Ahramat Nile Branch. Commun. Earth Environ. 5 (1), 233.

Gianessi, S., Polo, M., Stevanato, L., Lunardon, M., Francke, T., Oswald, S.E., Said Ahmed, H., Toloza, A., Weltin, G., Dercon, G., Fulajtar, E., Heng, L., Baroni, G., 2024. Testing a novel sensor design to jointly measure cosmic-ray neutrons, muons and gamma rays for non-invasive soil moisture estimation. Geosci. Instrum. Method. Data Syst. 13, 9–25. https://doi.org/10.5194/gi-13-9-2024.

Gomes, L., Beucher, A., Møller, A.B., Iversen, B., Børgesen, C., Adetsu, D., Sechu, G., Goswin, H., Koch, J., Adhikari, K., Knadel, M., Lamandé, M., Greve, M., Jensen, N., Gutierrez, S., Balstrøm, T., Koganti, T., Roell, Y., Peng, Y., Greve, M., 2023. Soil assessment in Denmark: towards soil functional mapping and beyond. Front. Soil Sci. 3, 1090145. https://doi.org/10.3389/fsoil.2023.1090145.

Goovaerts, P., 2017. Geostatistical Interpolation of Rate Data Using Poisson Kriging. In: Shekhar, S., Xiong, H., Zhou, X. (eds) Encyclopedia of GIS. Springer, Cham. Doi: 10.1007/978-3-319-17885-1_1642.

Gozukara, G., Hartemink, A.E., Huang, J., Demattê, J.A.M., 2025. Prediction accuracy of pXRF, MIR, and Vis-NIR spectra for soil properties—a review. Soil Sci. Soc. Am. J. 89, e70028. https://doi.org/10.1002/saj2.70028.

Granger, C.W.J., Ramanathan, R., 1984. Improved methods of combining forecasts. J. Forecast. 3, 197–204. https://doi.org/10.1002/for.3980030207.

Greenberg, I., Vohland, M., Seidel, M., Hutengs, C., Bezard, R., Ludwig, B., 2023. Evaluation of mid-infrared and X-ray fluorescence data fusion approaches for prediction of soil properties at the field scale. Sensors 23, 662. https://doi.org/10.3390/S23020662.

Grunwald, S., Murad, M.O.F., Farrington, S., Wallace, W., Rooney, D., 2024. Multi-sensor soil probe and machine learning modeling for predicting soil properties. Sensors 24 (21), 6855.

Guerrero, C., Wetterlind, J., Stenberg, B., Mouazen, A.M., Gabarrón-Galeote, M.A., Ruíz-Sinoga, J.D., Zornora, R., Viscarra Rossel, R.A., 2016. Do we really need large spectral libraries for local scale SOC assessment with NIR spectroscopy? Soil Tillage Res. 155, 501–509. https://doi.org/10.1016/j.still.2015.07.008.

Guerrero, C., Lorenzetti, R., 2021. Use of composite samples and NIR spectroscopy to detect changes in SOC contents. Geoderma 396, 115069. https://doi.org/10.1016/j.geoderma.2021.115069.

He H., Zou. W., Jones S. B., Robinson D. A., Horton R., Dyck. M., Filipović V., Noborio K., Bristow K., Gong Y., Sheng W., Wu Q., Feng H., Liu Y., 2023. Chapter Four - Critical review of the models used to determine soil water content using TDR-measured apparent permittivity (D. L. Sparks. Ed., Vol. 182. pp. 169–219). Academic Press. Doi: 10.1016/bs.agron.2023.06.004.

Hedley, C., Yule, I., Eastwood, C., Shepherd, T., Arnold, G., 2004. Rapid identification of soil textural and management zones using electromagnetic induction sensing of soils. Soil Res. 42, 389–400.

Hengl, T., Consoli, D., Tian, X., Nauman, T.W., Nussbaum, M., Isik, M.S., Harris, N., 2025. OpenLandMap-soildb: global soil information at 30 m spatial resolution for

2000–2022+ based on spatiotemporal Machine Learning and harmonized legacy soil samples and observations. Earth Syst. Sci. Data Discuss. 2025, 1–66.
Hong, Y., Liu, Yaolin, Chen, Y., Liu, Yanfang, Yu, L., Liu, Yi, Cheng, H., 2019. Application of fractional-order derivative in the quantitative estimation of soil organic matter content through visible and near-infrared spectroscopy. Geoderma 337, 758–769. https://doi.org/10.1016/j.geoderma.2018.10.025.
Horta, A., Acevedo, L., Neves, J., Soares, A., Pozza, L., 2021. Integrating portable X-ray fluorescence (pXRF) measurement uncertainty for accurate soil contamination mapping. Geoderma 382, 114712. https://doi.org/10.1016/j.geoderma.2020.114712.
Huang, J., Koganti, T., Santos, F.A.M., Triantafilis, J., 2017. Mapping soil salinity and a fresh-water intrusion in three-dimensions using a quasi-3d joint-inversion of DUALEM-421S and EM34 data. Sci. Total Environ. 577, 395–404.
Huisman, J., Sperl, C., Bouten, W., Verstraten, J., 2001. Soil water content measurements at different scales: accuracy of time domain reflectometry and ground-penetrating radar. J. Hydrol. 245, 48–58.
Hutengs, C., Eisenhauer, N., Schädler, M., Cesarz, S., Lochner, A., Seidel, M., Vohland, M., 2024. Enhanced VNIR and MIR proximal sensing of soil organic matter and PLFA-derived soil microbial properties through machine learning ensembles and external parameter orthogonalization. Geoderma 450, 117037.
James, G., Witten, D., Hastie, T., Tibshirani, R., 2021. An Introduction to Statistical Learning. Springer, New York, NY, USA.
Javadi, S.H., Munaff, M.A., Mouazen, A.M., 2021. Fusion of Vis-NIR and XRF spectra for estimation of key soil attributes. Geoderma 385 (2021), 114851. https://doi.org/10.1016/j.geoderma.2020.114851.
Ji W., Adamchuk V.I., Chen S., Mat Su A.S, Ismail A., Gan Q., Shi Z., Biswas A., 2019. Simultaneous measurement of multiple soil properties through proximal sensor data fusion: A case study, Geoderma, Volume 341,2019, Pages 111-128, ISSN 0016-7061, Doi: 10.1016/j.geoderma.2019.01.006.
Jenkins, R., Gould, R.W., Gedcke, D., 1995. Quantitative X-ray Spectrometry. CRC Press.
Jones, S.B., Wraith, J.M., Or, D., 2002. Time domain reflectometry measurement principles and applications. Hydrol. Process. 16 (1), 141–153. https://doi.org/10.1002/hyp.513.
Kerry, R., Escolà, A., 2021. Conclusions: Future directions in sensing for precision agriculture. In: Kerry, R., Escolà, A. (Eds.), *Sensing Approaches for Precision Agriculture* (pp. 399–407). Springer. Doi: 10.1007/978-3-030-78431-7_14.
Klotzsche, A., Jonard, F., Looms, M.C., van der Kruk, J., Huisman, J.A., 2018. Measuring soil water content with ground penetrating radar: a decade of progress. Vadose Zone J. 17, 180052.
Knadel, M., Castaldi, F., Barbetti, R., Ben-Dor, E., Gholizadeh, A., Lorenzetti, R., 2023. Mathematical techniques to remove moisture effects from visible–near-infrared–shortwave-infrared soil spectra — review. Appl. Spectrosc. Rev. 629–662. https://doi.org/10.1080/05704928.2022.2128365.
Knadel, M., Thomsen, A., Greve, M.H., 2011. Multisensor on-the-go mapping of soil organic carbon content. SSSAJ. Pedology. 75 (7), 1799–1806. https://doi.org/10.2136/sssaj2010.0452.
Knadel, M., Thomsen, A., Schelde, K., Greve, M.H., 2015. Soil organic carbon and particle sizes mapping using vis–NIR. EC and temperature mobile sensor platform. Comput. Electron. Agric. 114, 134–144. https://doi.org/10.1016/j.compag.2015.03.013.
Koganti, T., Van De Vijver, E., Allred, B.J., Greve, M.H., Ringgaard, J., Iversen, B.V., 2020. Mapping of agricultural subsurface drainage systems using a frequency-domain ground penetrating radar and evaluating its performance using a single-frequency multi-receiver electromagnetic induction instrument. Sensors 20 (14), 3922.
Koganti T., Vigah Adetsu D., Triantafilis J., Greve M.H., Breucher A. M. Mapping peat depth using a portable gamma-ray sensor and terrain attributes (2023). Geoderma 439, 116672. DOI: 10.1016/j.geoderma.2023.116672.
Kweon G., Lund E. D., Maxton C., Drummond S. T. and Jensen K., 2008. In Situ Measurement of Soil Properties Using a Probe-Based VIS- NIR Spectrophotometer. In: An ASABE Annual International Meeting Presentation. Rhode Island. doi: 10.13031/2013.24772.
Li, S., Viscarra Rossel, R.A., Webster, R., 2022. The cost-effectiveness of reflectance spectroscopy for estimating soil organic carbon. Eur. J. Soil Sci. 73 (1), e13202. https://doi.org/10.1111/ejss.13202.
Liu, W., Baret, F., Gu, X., Tong, Q., Zheng, L., Zhang, B., 2003. Evaluation of methods for soil surface moisture estimation from reflectance data. Int. J. Remote Sens. 24, 2069–2208.
Liu X., Dong X., Leskovar D.I., 2016. Ground penetrating radar for underground sensing in agriculture: A review. International Agrophysics 30. Soil organic matter, nitrogen and pH driven change in bacterial community following forest conversion,Forest Ecology and Management, Volume 477, 2020, 118473, ISSN 0378-1127, Doi: 10.1016/j.foreco.2020.118473.
Liu, S., Shen, H., Chen, S., Zhao, X., Biswas, A., Jia, X., Fang, J., 2019. Estimating forest soil organic carbon content using vis-NIR spectroscopy: Implications for large-scale soil carbon spectroscopic assessment. Geoderma 348, 37–44.
Loria, N., Lal, R., Chandra, R., 2024. Handheld in situ methods for soil organic carbon assessment. Sustainability 16 (13), 5592.
Lund E.D., Adamchuk V.I., Collings. K.L., Drummond P.E., Christy C.D., 2005. Development of soil pH and lime requirement maps using on-the-go soil sensors. In: The 5th European Conference on Precision Agriculture proceedings. J. Stafford (eds.). Wageningen. The Netherlands. pp. 457-464. Wageningen Academic Publishers. Doi: 10.3920/9789086865499_057.
Malone B., Stockmann U., Glover M., McLachlan G., Engelhardt S., Tuomi S., 2022. Digital soil survey and mapping underpinning inherent and dynamic soil attribute condition assessments,Soil Security, Volume 6,100048, ISSN 2667-0062, Doi: 10.1016/j.soisec.2022.100048.
Minasny, B., McBratney, A.B., 2025. Machine learning and artificial intelligence applications in soil science. Eur. J. Soil Sci. 76 (2). https://doi.org/10.1111/ejss.70093.
Møller, A.B., Koganti, T., Beucher, A., Iversen, B.V., Greve, M.H., 2021. Downscaling digital soil maps using electromagnetic induction and aerial imagery. Geoderma 385, 114852. https://doi.org/10.1016/j.geoderma.2020.114852.
Morgan, C.L.S., Waiser, T.H., Brown, D.C., Hallmark, C.T., 2009. Simulated in situ characterization of soil organic and inorganic carbon with visible near-infrared diffuse reflectance spectroscopy, Geoderma, 151(3–4). ISSN 249–256, 0016–7061. https://doi.org/10.1016/j.geoderma.2009.04.010.
McBratney, A.B., Minasny, B., Malone, B.P., 2011a. Characterizing soils using a portable X–ray fluorescence spectrometer: 1. Soil Texture. Geoderma 167–168, 167–177. https://doi.org/10.1016/j.geoderma.2011.08.010.
McBratney, A.B., Minasny, B., Whelan, B., 2011a. Defining proximal soil sensing. In: Adamchuk, V.I., Viscarra Rossel, R.A. (Eds.), The Second Global Workshop on Proximal Soil Sensing. McGill University, Montreal, pp. 144–146.
McBratney A.B., Mendonça Santos M.L., Minasny B., 2003. On digital soil mapping, Geoderma, Volume 117, Issues 1–2, Pages 3-52, ISSN 0016-7061, Doi: 10.1016/S0016-7061(03)00223-4.
McBride, M.B., 2022. Estimating soil chemical properties by diffuse reflectance spectroscopy: promise versus reality. Eur. J. Soil Sci. 73 (1), e13192. https://doi.org/10.1111/ejss.13192.
Næs, T.; Isakson, T.; Fearn, T.; Davies, T.; Ziegel, E.R. A (2004). User-Friendly Guide to Multivariate Calibration and Classification; NIR Publications: Charlton, Chichester, UK,; Volume 46; ISBN 1906715254.
McNeill J.D., 1980. Electromagnetic terrain conductivity measurement at low induction numbers. Technical Note TN-6. Mississauga. ON.Canada: Geonic Ltd.
Muñoz-Carpena R., Ritter A., Bosch D., 2005. Field methods for monitoring soil water status. In J. Alvarez-Benedi., R. Munoz-Carpena (Eds). Soil-Water-Solute Process Characterization an Integrated Approach (pp. 167–195). CRC Press.
Musa, P., Sugeru, H., Wibowo, E.P., 2024. Wireless sensor networks for precision agriculture: a review of NPK sensor implementations. Sensors 24 (1), 51. https://doi.org/10.3390/s24010051.
Najdenko, E., Lorenz, F., Dittert, K., Olfs, H.W., 2024. Rapid in-field soil analysis of plant-available nutrients and pH for precision agriculture—A review. Precision Agriculture, 25(6), 3189-3218.
Næs, T., Brockhoff, P.B., Tomic, O., 2010. Statistics for Sensory and Consumer Science. Wiley. https://doi.org/10.1002/9780470669181.
Niemeyer, J., Chen, Y., Bollag, J.M., 1992. Characterization of humic acids. Composts and peat by diffuse reflectance fourier transform infrared spectroscopy. Soil Sci. Soc. Am. J. 56 (1), 135–140.
Nortcliff, S., 2002. Standardisation of soil quality attributes. Agr Ecosyst Environ 88 (2), 161–168. https://doi.org/10.1016/S0167-8809(01)00253-5.
Oliver, M.A., 2010. An Overview of Geostatistics and Precision Agriculture. In: Oliver, M. (eds) Geostatistical Applications for Precision Agriculture. Springer, Dordrecht. Doi: 10.1007/978-90-481-9133-8_1.
O'Rourke, S.M., Minasny, B., Holden, N.M., McBratney, A.B., 2016. Synergistic use of vis-NIR. MIR. and XRF spectroscopy for the determination of soil geochemistry. Soil Sci. Soc. Am. J. 80, 888–899.
Page, M.J., McKenzie, J.E., Bossuyt, P.M., Boutron, I., Hoffmann, T.C., Mulrow, C. D., et al., 2021. The PRISMA 2020 statement: an updated guideline for reporting systematic reviews. BMJ, 372.
Parry, L.E., West, L.J., Holden, J., Chapman, P.J., 2014. Evaluating approaches for estimating peat depth. J. Geophys. Res. Biogeo. 119 (4), 567–576.
Pathirana, S., Lambot, S., Krishnapillai, M., Cheema, M., Smeaton, C., Galagedara, L., 2023. Ground-penetrating radar and electromagnetic induction: challenges and opportunities in agriculture. Remote Sens. (Basel) 15 (11), 2932.
Pedrera-Parrilla, A., Van De Vijver, E., Van Meirvenne, M., Espejo-Perez, A.J., Giraldez, J.V., Vanderlinden, K., 2016. Apparent electrical conductivity measurements in an olive orchard under wet and dry soil conditions: significance for clay and soil water content mapping. Precis. Agric. 17, 531–545.
Pepers, K.H.J., van Egmond, F., Koomans, R., Teuling, K., Staats, G., van Os, G., 2024. Validation of a new gamma ray soil bulk density sensor. Eur. J. Soil Sci. 75 (4), e13542. https://doi.org/10.1111/ejss.13542.
Perčin, A., Hefer, H., Zgorelec, Ž., Galić, M., Rašić, D., Kisić, I., 2025. Evaluation of agricultural soil quality and associated human health risks following plastic fire incidents: insights from a case study. Land 14 (11), 2137. https://doi.org/10.3390/land14112137.
Piccini, C., Metzger, K., Debaene, G., Stenberg, B., Götzinger, S., Boruvka, L., Sandén, T., Bragazza, L., Liebisch, F., 2024. In-field soil spectroscopy in Vis-NIR range for fast and reliable soil analysis: a review. Eur. J. Soil Sci. 75, 13481. https://doi.org/10.1111/ejss.13481.
Piikki K., Söderström M., 2019. Digital soil mapping of arable land in Sweden – Validation of performance at multiple scales, Geoderma,Volume 352, Pages 342-350, ISSN 0016-7061, Doi: 10.1016/j.geoderma.2017.10.049.
Porto, P., Fulajtar, E., Walling, D. E., Callegari, G., Cogliandro, V., La Spada, C., et al., 2024. Geographical Overview of 137Cs Resampling Studies. In: Using 137Cs Resampling Method to Estimate Mean Soil Erosion Rates for Selected Time Windows (pp. 15-109). Cham: Springer Nature Switzerland.
Potts, P.J., Sargent, M., 2022. In situ measurements using hand-held XRF spectrometers: a tutorial review. J. Anal. At. Spectrom 37 (10), 1928–1947. https://doi.org/10.1039/D2JA00171C.

Priori, S., Barbetti, R., Meini, L., Morelli, A., Zampolli, A., D'avino, L., 2019. Towards economic land evaluation at the farm scale based on soil physical-hydrological features and ecosystem services. Water 11 (8), 1527.
Ramirez-Lopez, L., et al., 2019. Soil spectral libraries in support of digital soil mapping. Geoderma 356, 113977.
Ramos, P.V., Inda, A.V., Barrón, V., Teixeira, D.D.B., Marques, J., 2021. Magnetic susceptibility in the prediction of soil attributes in southern Brazil. Soil Sci. Soc. Am. J. 85 (1), 102–116. https://doi.org/10.1002/saj2.20164.
Ravansari, R., Wilson, S.C., Tighe, M., 2020. Portable X-ray fluorescence for environmental assessment of soils: not just a point and shoot method. Environ. Int. 134. https://doi.org/10.1016/j.envint.2019.105250.
Reynolds J.M., 1997. Ground penetrating radar. An introduction to applied and environmental geophysics. John Wiley., Sons. Chichester. pp. 681-749.
Rosso, P., Huang, S., Inforsato, L., et al., 2025. Combining mobile proximal soil sensors and a crop model to produce high spatial resolution yield prediction maps. Precis. Agric. 26, 79. https://doi.org/10.1007/s11119-025-10274-w.
Roth, K., Schulin, R., Flühler, H., Attinger, W., 1990. Calibration of time domain reflectometry for water content measurement using a composite dielectric approach. Water Resour. Res. 26 (10), 2267–2273. https://doi.org/10.1029/WR026i010p02267.
Saey, T., Simpson, D., Vermeersch, H., Cockx, L., Van Meirvenne, M., 2009. Comparing the EM38DD and DUALEM-21S sensors for depth-to-clay mapping. Soil Sci. Soc. Am. J. 73 (1), 7–12.
Sanderman, J., Savage, K., Dangal, R.S., 2019. Mid-infrared spectroscopy for prediction of soil health indicators in the United States. Soil Sci. Soc. Am. J. 84 (1), 251–261. https://doi.org/10.1002/saj2.20009.
Shackley, M. S. (Ed.)., 2010. X-ray fluorescence spectrometry (XRF) in geoarchaeology. Springer New York.
Schmidinger, J., Barkov, V., Tavakoli, H., Correa Reyes, J., Ostermann, M., Atzmüller, M., Gebbers, R., Vogel, S., 2024. Which and how many soil sensors are ideal to predict key soil properties: a case study with seven sensors. Geoderma 450, 117017. https://doi.org/10.1016/j.geoderma.2024.117017.
Shirzaditabar, F., Heck, R.J., 2022. Characterization of soil magnetic susceptibility: a review of fundamental concepts, instrumentation, and applications. Can. J. Soil Sci. 102 (2), 231–251. https://doi.org/10.1139/CJSS-2021-0040.
Söderström, M., Eriksson, J., 2013. Gamma-ray spectrometry and geological maps as tools for cadmium risk assessment in ara.
Song, J., Shi, X., Wang, H., Lv, X., Zhang, W., et al., 2024. Combination of feature selection and geographical stratification increases the soil total nitrogen estimation accuracy based on vis-NIR and pXRF spectral fusion. Comput. Electron. Agric. 212, 108636. https://doi.org/10.1016/j.compag.2024.108636.
Stenberg, B., Koganti, T., Castaldi, F., Metzger, K., Buttafuoco, G., van Egmond, F., Cayuela, J. A., Borůvka, L., Debaene, G., Liebisch, F., Sandén, T., 2024. D5.1 ProbeField: Best Practice Protocol for Field Spectroscopy and Assessment by Soil Spectral Library Based Calibrations (Ver 1). Zenodo. Doi: 10.5281/zenodo.14150972.
Stenberg, B., 2010. Effects of soil sample pretreatments and standardised rewetting as interacted with sand classes on Vis-NIR predictions of clay and soil organic carbon. Geoderma 158 (1–2), 15–22.
Stenberg, B., Viscarra Rossel, R.A., Mouazen, A.M., Wetterlind, J., 2010. Visible and near infrared spectroscopy in soil science. Adv. Agron. 107, 163–215.
Sudduth, K.A., Drummond, S.T., Kitchen, N.R., 2001. Accuracy issues in electromagnetic induction sensing of soil electrical conductivity for precision agriculture (2001). Comput. Electron. Agricult.. 31 (3). 239-264. DOI: Doi: 10.1016/S0168-1699(00)00185-X.
Sudduth, K.A., Hummel, J., 1996. Geographic operating range evaluation of a NIR soil sensor. Trans. ASABE 39, 1599–1604.
Tabatabai, S., Knadel, M., Thomsen, A., Greve, M.H., 2019. On-the-go sensor fusion for prediction of clay and organic carbon using pre-processing survey. different validation methods. and variable selection. Soil Sci. Soc. Am. J. 83, 300–310. https://doi.org/10.2136/sssaj2018.10.0377.
Tavares, T.R., Minasny, B., McBratney, A., Cherubin, M.R., Marques, G.T., Ragagnin, M. M., Alves, E.E.N., Padarian, J., Lavres, J., Pereira de Carvalho, H.W., 2023. Estimating plant-available nutrients with XRF sensors: towards a versatile analysis tool for soil condition assessment. Geoderma 439, 116701. https://doi.org/10.1016/j.geoderma.2023.116701.
Tavares, T.R., Molin, J.P., Javadi, S.H., Carvalho, H.W.P.D., Mouazen, A.M., 2020. Combined use of vis-NIR and XRF sensors for tropical soil fertility analysis: Assessing different data fusion approaches. Sensors 21 (1), 148.
Taylor, J.A., McBratney, A.B., Viscarra Rossel, R.A., Minasny B., Taylor H., Whelan B., Short M., 2006. Development of a multi-sensor platform for proximal soil sensing. Philadelphia. 18th World Congress of Soil Science. Pennsylvania. USA.
Topp, G.C., Davis, J.L., Annan, A.P., 1980. Electromagnetic determination of soil water content: measurements in coaxial transmission lines. Water Resour. Res. 16 (3), 574–582. https://doi.org/10.1029/WR016i003p00574.
Tóth, T., Kovács, Z.A., Rékási, M., 2019. XRF-measured rubidium concentration is the best predictor variable for estimating the soil clay content and salinity of semi-humid soils in two catenas. Geoderma 342, 106–108. https://doi.org/10.1016/j.geoderma.2019.02.011.
Towett, E.K., Shepherd, K.D., Sila, A., Aynekulu, E., Cadisch, G., 2015. Mid-infrared and total x-ray fluorescence spectroscopy complementarity for assessment of soil properties. Soil Sci. Soc. Am. J. 79 (5), 1375–1385.
Triantifilis, J., Feiko, V.Z., McNally, S., Kumar, K., Ekanayake, J., McNeill, S., 2024. Where Can One Bury One's Soil Carbon, Using a Digital Soil Mapping Approach?. https://doi.org/10.2139/ssrn.4760326.
Tu, Y., Tang, H., Hu, W., 2022. An application of a LPWAN for upgrading proximal soil sensing systems. Sensors 22 (12), 4333.
Tziolas, N., Tsakiridis, N., Ben-Dor, E., Theocharis, J., Zalidis, G., 2019. A memory-based learning approach utilizing combined spectral sources and geographical proximity for improved VIS-NIR-SWIR soil properties estimation. Geoderma 340, 11–24.
USEPA (United States Environmental Protection Agency), 2007. Method 3051a (SW-846): Microwave assisted acid digestion of sediments, sludges, soils and oils. https://www.epa.gov/sites/production/files/2015-12/documents/3051a.pdf. (Acessed 28 jun. 2023).
USEPA (United States Environmental Protection Agency), 2007. Method 6200; Field Portable X-ray Fluorescence Spectrometry for the Determination of Elemental Concentrations in Soil and Sediment. Washington. DC. USA. https://www.epa.gov/sites/default/files/2015-12/documents/6200.pdf (Acessed 28 jun. 2023).
van der Graaf, E.R., Koomans, R.L., Limburg, J., de Vries, K., 2007. In situ radiometric mapping as a proxy of sediment contamination: Assessment of the underlying geochemical and -physical principles. Appl. Radiat. Isot. 65 (5), 619–633. https://doi.org/10.1016/j.apradiso.2006.11.004.
van Egmond, F.M., Loonstra, E.H., Limburg, J., 2010. Gamma ray sensor for topsoil mapping: The Mole. In: Proximal Soil Sensing. Progress in Soil Science. Springer. Vol.1. 323-332.
van Egmond, F.M., van der Veeke, S., Knotters, M., Koomans, R.I., Walvoort, D.J.J., Limburg, J., 2018. Mapping soil texture with a gamma-ray spectrometer: comparison between UAV and proximal measurements and traditional sampling: validation study. (WOt-technical report; No. 137). WOT Natuur, Milieu. Doi: 10.18174/466037.
van Egmond, F., Liebisch, F., Metzger, K., Sandén, T., Koganti, T., Borůvka, L., Stenberg, B., 2024. Decision trees to assist soil sensing measurement choices. Proceedings of the GPSS workshop 2024.
Vanhoof, C., Bacon, J.R., Fittschen, U.E.A., Vincze, L., 2022. Atomic spectrometry update: review of advances in X-ray fluorescence spectrometry and its special applications. J. Anal. At. Spectrom 37 (9), 1761–1775. https://doi.org/10.1039/D2JA90035A.
Vasques, G.M., Rodrigues, H.M., Coelho, M.R., Baca, J.F.M., Dart, R.O., Oliveira, R.P., Teixeira, W.G., Ceddia, M.B., 2020. Field proximal soil sensor fusion for improving high-resolution soil property maps. Soil Systems 4 (3), 52. https://doi.org/10.3390/soilsystems4030052.
Wangeci, A., Knadel, M., De Pascale, O., Greve, M.H., Senesi, G.S., 2024. Assessing the performance of handheld LIBS for predicting soil organic carbon and texture in European soils. J. Anal. At. Spectrom 39 (11), 2903–2916.
Veum, K.S., Sudduth, K.A., Kremer, R.J., Kitchen, N.R., 2017. Sensor data fusion for soilhealth assessment. Geoderma 305, 53–61. https://doi.org/10.1016/j.geoderma.2017.05.031.
Veum, K.S., Sudduth, K.A., Kremer, R.J., Kitchen, N.R., 2015. Estimating a soil quality index with VIS-NIR reflectance spectroscopy. Soil Sci. Soc. Am. J. 79, 637–649. https://doi.org/10.2136/sssaj2014.09.0390.
Viscarra Rossel, R.A., McBratney, A.B., 1998. Laboratory evaluation of a proximal sensing technique for simultaneous measurement of soil clay and water content. Geoderma 85 (1), 19–39.
Viscarra Rossel, R.A., Taylor, H.J., McBratney, A.B., 2007. Multivariate calibration of hyperspectral γ-ray energy spectra for proximal soil sensing. Eur. J. Soil Sci. 1, 343–353.
Viscarra Rossel, R.A., Rizzo, R., Demattê, J.A., Behrens, T., 2010. Spatial modeling of a soil fertility index using visible-near-infrared spectra and terrain attributes. Soil Sci. Soc. Am. J. 74, 1293–1300. https://doi.org/10.2136/sssaj2009.0130.
Viscarra Rossel, R.A., Adamchuk, V., Suddut, K., McKenzie, N., Lobsey, C., 2011. Proximal soil sensing: an effective approach for soil measurements in space and time. Adv. Agron. 113 (113), 237–282. https://doi.org/10.1016/B978-0-12-386473-4.00010-5.
Viscarra Rossel, R.A., et al., 2016. A global spectral library to characterize the world's soil. Earth Sci. Rev. 155, 198–230.
Viscarra Rossel, R. A., Shen, Z., Ramirez-Lopez, L., Behrens, T., Shi, Z., Wetterlind, J., Sudduth, K. A., Stenberg, B., Guerrero, C., Gholizadeh, A., Ben-Dor, E., St. Luce, M., Orellano, C., 2024. An imperative for soil spectroscopic modelling is to think global but fit local with transfer learning. Earth-Science Reviews, 254, Article 104797. Doi: 10.1016/j.earscirev.2024.104797.
Wang, D., Chakraborty, S., Weindorf, D.C., Li, B., Sharma, A., Paul, S., Ali, M.N., 2015. Synthesized use of VisNIR DRS and PXRF for soil characterization: Total carbon and total nitrogen. Geoderma 243–244, 157–167.
Wang, S., Li, W., Li, J., Liu, X., 2013. Prediction of soil texture using FT-NIR spectroscopy and PXRF spectrometry with data fusion. Soil Sci. 178, 626–638.
Weindorf, D.C., Chakraborty, S., Herrero, J., Li, B., Castañeda, C., Choudhury, A., 2016. Simultaneous assessment of key properties of arid soil by combined PXRF and Vis-NIR data. Eur. J. Soil Sci. 67, 173–183.
Wetterlind, J., Viscarra Rossel, R.A., Steffens, M., 2022. Diffuse reflectance spectroscopy characterises the functional chemistry of soil organic carbon in agricultural soils. Eur. J. Soil Sci. 73 (4), e13263. https://doi.org/10.1111/ejss.13263.
White I., Zegelin S.J., 1995. Electric and Dielectric Methods for Monitoring Soil-Water Content. In: L. G. Wilson L. G. Everett S. J. Cullen (Eds). Handbook of Vadose Zone Characterization., Monitoring (pp. 343–385). CRC Press. Doi: 10.1201/9780203752524.
Wigneron, J.P., Jackson, T.J., O'Neill, P.E., De Lannoy, G., de Rosnay, P., Walker, J.P., Ferrazzoli, P., Mironov, V., Bircher, S., Grant, J.P., Kurum, M., Schwank, M., Muñoz-Sabater, J., Das, N., Royer, A., Al-Yaari, A., Al Bitar, A., Fernandez-Moran, R., Lawrence, H., Kerr, Y.H., 2017. Modelling the passive microwave signature from land surfaces: a review of recent results and application to the L-band SMOS & SMAP

soil moisture retrieval algorithms. Remote Sens. Environ. 192, 238–262. https://doi.org/10.1016/j.rse.2017.01.024.
Williams, P., Norris K., 2001 Near-Infrared Technology in the Agricultural and Food Industries. American Association of Cereal Chemists, USA.
Wu, K., Lambot, S., 2022. Analysis of low-frequency drone-borne GPR for root-zone soil electrical conductivity characterization. IEEE Trans. Geosci. Remote Sens. 60, 1–13.
Wu, K., Rodriguez, G.A., Zajc, M., Jacquemin, E., Clément, M., De Coster, A., Lambot, S., 2019. A new drone-borne GPR for soil moisture mapping. Remote Sens. Environ. 235, 111456.
Xia, F., Hu, B., Shao, S., Xu, D., Zhou, Y., Zhou, Y., Huang, M., Li, Y., Chen, S., Shi, Z., 2019. Improvement of spatial modeling of Cr, Pb, Cd, As and Ni in soil based on portable X-ray fluorescence (PXRF) and geostatistics: a case study in east China. Int. J. Environ. Res. Public Health 16, 2694. https://doi.org/10.3390/ijerph16152694.
Yang, P., Mao, R., Zhao, J., Zhang, Y., 2007. Spatial variability of soil magnetic susceptibility under different water qualities for irrigation. Trans. Chinese Soc. Agricult. Eng. 23 (6), 12–16.
Yurui, S., Lammers, P.S., Daokun, M., Jianhui, L., Qingmeng, Z., 2008. Determining soil physical properties by multi-sensor technique. Sens. Actuators, A 147 (1), 352–357. https://doi.org/10.1016/j.sna.2008.05.014.
Zare, E., Huang, J., Santos, F.A.M., Triantafilis, J., 2015. Mapping salinity in three dimensions using a DUALEM-421 and electromagnetic inversion software. Soil Sci. Soc. Am. J. 79, 1729–1740. https://doi.org/10.2136/sssaj2015.06.0238.
Zare, E., Arshad, M., Zhao, D., Nachimuthu, G., Triantafilis, J., 2020. Two-dimensional time-lapse imaging of soil wetting and drying cycle using EM38 data across a flood irrigation cotton field. Agric Water Manag 241, 106383. https://doi.org/10.1016/j.agwat.2020.106383.
Zhang, J., Lin, H., Doolittle, J., 2014. Soil layering and preferential flow impacts on seasonal changes of GPR signals in two contrasting soils. Geoderma 213, 560–569.
Zhang, X., Feng, G., Sun, X., 2024. Advanced technologies of soil moisture monitoring in precision agriculture: a review. J. Agricult. Food Res. 18, 101473.
Zhang, Y., Ji, W., Saurette, D.D., Easher, T.H., Li, H., Shi, Z., Adamchuk, V.I., Biswas, A., 2020. Three-dimensional digital soil mapping of multiple soil properties at a field-scale using regression kriging. Geoderma 366, 114253. https://doi.org/10.1016/j.geoderma.2020.114253.
Zhao, X., Wang, J., Zhao, D., Li, N., Zare, E., Triantafilis, J., 2019. Digital regolith mapping of clay across the Ashley irrigation area using electromagnetic induction data and inversion modelling. Geoderma 346, 18–29. https://doi.org/10.1016/j.geoderma.2019.01.033.
Zhong, L., Guo, X., Xu, Z., Ding, M., 2021. Soil properties: their prediction and feature extraction from the LUCAS spectral library using deep convolutional neural networks. Geoderma 402, 115366.
Zhou, Y., Ferdinand, M.S., van Wesemael, J., Dvorakova, K., Baret, P.V., Van Oost, K., van Wesemael, B., 2025. A framework for mapping conservation agricultural fields using optical and radar time series imagery. Remote Sens. Environ. 328, 114858. https://doi.org/10.1016/j.rse.2025.114858.